AGSO Journal of Australian Geology & Geophysics, 16(5), 637–654

Zircon U–Pb ages and geochemistry of igneous and metamorphic rocks in the northern Prince Charles Mountains, Antarctica

P.D. Kinny[1], L.P. Black[2], & J.W. Sheraton[2]

High-grade metamorphic and felsic igneous rocks from the northern Prince Charles Mountains, East Antarctica, have been characterised geochemically and dated from SHRIMP zircon geochronological data. Around 980 Ma ago, voluminous magmas representing a combination of mantle-derived and intracrustal melts, including orthopyroxene–quartz monzonite ('charnockite') on Loewe Massif and granitic and syenitic intrusions on Mount Collins, were emplaced during a regional high-grade tectonothermal event. Garnet leucogneiss sheets on Mount McCarthy, the products of local partial melting, were also emplaced at about this time. The geology of Fisher Massif is exceptional in that a ca 1280-Ma metavolcanic sequence and coeval granodiorite have been metamorphosed only up to the lower amphibolite facies, and intruded by a ca 1020-Ma biotite granite. None of the analysed samples shows in its isotopic systematics the effects of 500-Ma events, prominent elsewhere in East Antarctica. Rare inherited components 1850–1900 Ma old were found in some samples. A paragneiss on Mount Meredith yielded 2500–2800-Ma and 1800–2100-Ma detrital zircon populations.

Introduction

The Prince Charles Mountains (PCM) occupy a vast (600 × 300 km) region of MacRobertson Land, East Antarctica. They extend from the head of the Lambert glacier (lat. 75°S) north to the Amery Ice Shelf (lat. 70°S) between longitudes 60 and 70°E. They comprise sharp peaks and steep-sided massifs rising to 1000 m above the local ice surface. Their more northerly exposures are dominated by granulite-facies rocks that are part of an extensive but sparsely exposed Meso- to Neoproterozoic basement. These rocks were previously correlated with the Rayner Complex of Enderby and Kemp Land, and basement rocks of the Mawson and Prydz Bay coastlines (Fig. 1). To the south, the rocks of the PCM are of lower metamorphic grade, and include Archaean granitic basement and probably Proterozoic metasedimentary cover sequences (Tingey 1982, 1991).

Fitzsimons & Thost (1992) described basement geological relationships in the northern PCM, specifically in the Athos, Porthos, and Aramis Ranges. The Porthos and Aramis Ranges are composed primarily of homogeneous felsic orthogneiss and intrusives enclosing minor mafic and ultramafic boudins and rare metasediments. In the Athos Range and on Jetty Peninsula, paragneiss is more abundant. Granulite-facies assemblages attributed to a regional 1000-Ma event indicate peak conditions of 0.6 to 0.7 GPa and 700 to 800°C (Fitzsimons & Thost 1992). Late in the metamorphic history, early flat-lying structures were redeformed into upright folds and shears, and discordant leucogneiss bodies (representing locally derived partial melts) and large orthopyroxene-bearing granite ('charnockite') plutons were emplaced (Fitzsimons & Thost 1992).

Farther south, the outcrops are geologically quite distinct from those in the more northerly ranges. Fisher Massif (Fig. 1), for example, comprises a low- to medium-grade metavolcanic sequence and granitic intrusions, and a layered metagabbro complex crops out on Mount Willing (Tingey 1982, 1991; Fedorov et al. 1987).

Other descriptions of geological relations in the northern PCM have been published recently by McKelvey & Stephenson (1990; Radok Lake area), Manton et al. (1992; Jetty Peninsula), Kamenev et al. (1993; summary of extensive mapping by Russian geologists throughout the PCM), and Hand et al. (1994; Else Platform).

By current standards, age relations in and around the PCM are poorly established. This paper seeks to redress this deficiency by presenting new U–Pb zircon geochronological data for ten samples collected from Mount McCarthy, Loewe Massif, Fisher Massif, Mount Collins, and Mount Meredith (Fig. 1) during the 1990–91 summer field season. Ages have been obtained via the SHRIMP ion-probe technique (Compston et al. 1984, 1992), for which analytical notes are presented in the Appendix. Geochemical data for all samples presented in Table 1 show that most are I-type granites (derived by the melting of igneous source rocks) according to the classification of Chappell & White (1974). These rocks are diopside- (Di) or only slightly corundum- (C) normative and have ASI (alumina saturation indices: atomic Al/[Na + K + Ca]) <1.1, which is consistent with the common occurrence of hornblende, titanite, and allanite. However, sample 91286403 from Mount McCarthy might be of S-type origin (derived by the melting of sedimentary source rocks), and samples 91286412 and 13 from Mount Meredith are paragneiss.

Previous geochronology

Arriens (1975) presented (and Tingey 1982, 1991 revised) reconnaissance Rb–Sr ages from across the PCM. His total-rock isochron ages in the northern PCM and northern parts of the southern PCM range from 550 to 1090 Ma; many are ca 1000 Ma. Biotite and muscovite evince ages of 400 to 660 Ma; most are clustered around 500 Ma. From these data, Tingey (1982) postulated a major metamorphic episode in the northern PCM about 1000 Ma ago, and a widespread 500-Ma thermal event that reset mineral isotope systems and generated cross-cutting granitic pegmatites and stocks.

In contrast, a large part of the area that Arriens sampled in the southern PCM preserves late Archaean Rb–Sr isochron ages, indicating the presence of a large Archaean craton and less isotopic disturbance by 1000-Ma events in that area. A map in Tingey (1982) shows an inferred inlier of Archaean basement characterised by tholeiitic dyke swarms in the area encompassing Fisher Massif, Mount Collins, and Mount Willing (northern PCM; Fig. 1). Tingey correlated these dykes with similar-looking dykes of probable Palaeo- to Mesoproterozoic age which cut the Archaean rocks of the southern PCM, but recent geochemical studies show that they are unrelated (J.W. Sheraton, unpublished data).

More recent geochronology on Jetty Peninsula and Else Platform (Manton et al. 1992) has yielded Rb–Sr mineral isochron and conventional U–Pb zircon ± monazite ages of granulite-facies gneiss, two suites of intrusive granitic rocks, and a pegmatite. Zircons from the gneiss gave a U–Pb concordia upper intercept age of 1000 + 14/–11 Ma, interpreted as dating the granulite-facies metamorphism. One of the granite suites (gneissic leucogranite) gave ages of 940 + 24/–17 Ma (U–Pb zircon) and 718 ± 32 Ma (Rb–Sr); the other (biotite granite) did not yield an interpretable zircon age, but gave Rb–Sr mineral isochron ages of ca 480 Ma, similar to the projected lower intercept ages of some of the zircon discordia. Monazites

[1] Department of Applied Physics, Curtin University of Technology, GPO Box U1987, Perth, Western Australia, 6001.
[2] Minerals Division, Australian Geological Survey Organisation, GPO Box 378, Canberra, ACT 2601.

from both granites yielded ages between 530 and 540 Ma. Concordant U–Pb ages ranging from 495 to 505 Ma were obtained from the pegmatite. Manton et al. (1992) also cited Pb-isotope ages ranging from 830 to 968 Ma (Yakovlev et al. 1986) for orthopyroxene-bearing rocks in the Jetty Peninsula–Radok Lake area.

Mikhalsky et al. (1992) reported an Sm–Nd isochron age of 1233 ± 160 Ma, and a ca 1000-Ma metamorphic resetting age for mineral separates from nine samples of the layered gabbronorite complex on Mount Willing. They also documented conventional U–Pb zircon data for three granitic rocks from Mount Collins, from which they interpreted a crystallisation age of 1400 ± 80 Ma and subsequent disturbances between 700 and 900 Ma. Beliatsky et al. (1994) presented conventional multigrain zircon U–Pb data for mixed samples of low-grade metavolcanic rocks from Fisher Massif. They obtained discordia ages from five fractions indicating igneous emplacement at ca 1300 Ma, and a much older discordant point with a $^{207}Pb/^{206}Pb$ age of ca 2560 Ma from a sample of rhyodacite interpreted as having a clastic component.

Hensen et al. (1992) reported an Rb–Sr whole-rock age of 882 ± 140 Ma for intrusive charnockitic rocks of the Porthos Range. More recently, Zhou & Hensen (1995) applied Sm–Nd dating of whole-rock–garnet pairs to a leucogneiss sheet at Mount McCarthy. They interpreted their isochron age of ca 1150 Ma as reflecting contamination by monazite inclusions in the garnet. After leaching of contaminants, the garnets gave ages ranging from 635 to 555 Ma. (In this paper we present zircon data for what appears to be the same generation of leucogneiss.) A nearby two-pyroxene granulite gave an age of ca 630 Ma by the same method.

Finally, Phanerozoic K–Ar ages have been obtained for a

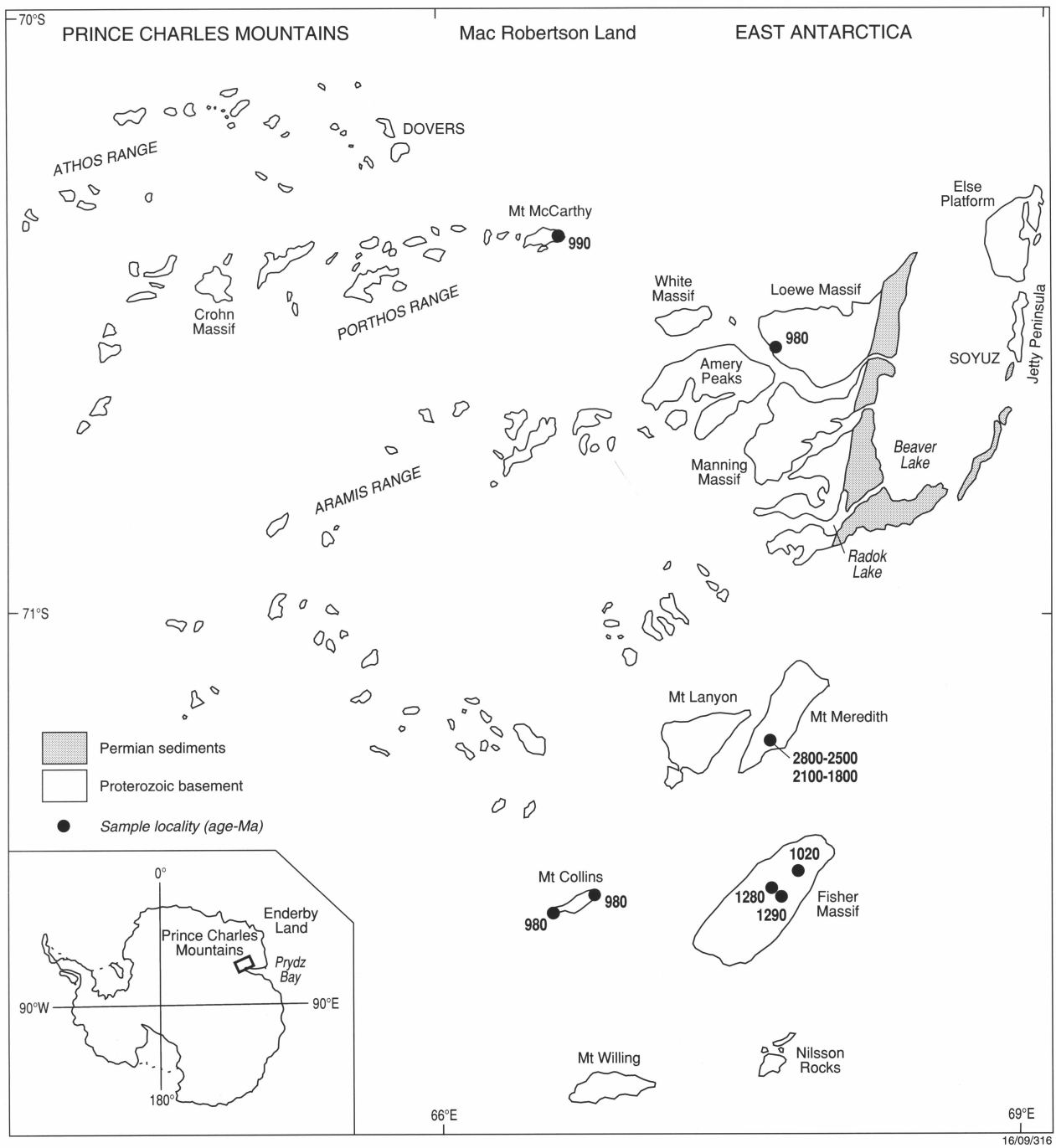

Figure 1. Sketch map of the northern PCM showing outcrops, sample localities (filled circles), and corresponding SHRIMP U–Pb zircon ages (Ma).

Table 1. Chemical analyses of dated samples.

Sample no.	*91286403*	*91286407*	*91286412*	*91286413*	*91286415*	*91286416*	*91286417*	*91286419*	*91286420*	*91286421*
Field no.	*MAC3*	*LOE7*	*MEM12*	*MEM13*	*FIR15*	*FIR16*	*FIR17*	*COL19*	*COL20*	*COL21*
Locality	*Mount McCarthy*	*Loewe Massif*	*Mount Meredith*	*Mount Meredith*	*Fisher Massif*	*Fisher Massif*	*Fisher Massif*	*Mount Collins*	*Mount Collins*	*Mount Collins*
Lithology	*Gt leuco-granite–gneiss*	*Bt-Hb-Op quartz monzonite*	*Bt-Kf-Qz-Pl gneiss*	*Bt-Pl psammite*	*Bt granite*	*Bt grano-diorite*	*Bt-Hb meta-dacite*	*Hb-Bt granite (foliated)*	*Hb-Bt granite*	*Cp quartz syenite*
SiO_2	76.28	58.92	70.27	86.23	67.11	72.60	64.75	64.44	74.55	58.66
TiO_2	0.02	1.57	0.53	0.26	0.51	0.27	0.53	0.59	0.21	0.81
Al_2O_3	12.41	15.11	13.86	6.25	15.04	13.43	13.02	15.72	12.45	17.80
Fe_2O_3	0.22	2.28	2.07	0.53	1.56	1.23	1.83	1.41	0.86	2.28
FeO	0.77	5.44	2.19	1.06	1.74	1.59	3.10	3.27	1.31	4.07
MnO	0.03	0.13	0.06	0.02	0.07	0.07	0.08	0.08	0.05	0.16
MgO	0.18	2.32	0.98	0.53	1.11	0.55	3.17	1.15	0.12	0.64
CaO	0.58	4.98	3.64	1.05	2.75	2.46	6.15	2.91	0.79	3.40
Na_2O	2.24	3.13	3.09	1.78	3.80	4.26	3.73	3.84	3.36	4.31
K_2O	6.19	3.71	1.36	0.72	3.85	1.72	0.37	4.37	5.44	5.89
P_2O_5	0.06	0.92	0.14	0.06	0.16	0.07	0.08	0.19	0.03	0.24
LOI	0.30	0.85	0.93	0.53	1.57	0.93	2.46	0.77	0.51	1.25
Rest	0.06	0.58	0.19	0.08	0.26	0.15	0.16	0.41	0.18	0.52
Total	**99.34**	**99.93**	**99.31**	**99.10**	**99.53**	**99.33**	**99.42**	**99.15**	**99.86**	**100.03**
	CIPW norms									
Q	37.65	12.90	37.52	69.74	22.63	34.62	25.05	16.24	31.94	2.17
C	1.11	–	1.02	0.78	–	0.26	–	–	–	–
Or	36.58	21.92	8.04	4.25	22.75	10.16	2.19	25.82	32.15	34.81
Ab	18.95	26.49	26.15	15.06	32.15	36.05	31.56	32.49	28.43	36.47
An	2.49	16.22	17.14	4.82	12.60	11.75	17.69	12.75	2.82	11.83
Di	–	2.05	–	–	–	–	9.92	0.37	0.78	2.97
Hy	1.70	10.51	3.99	2.43	3.96	2.96	6.55	6.69	1.33	4.62
Mt	0.32	3.31	3.00	0.77	2.26	1.78	2.65	2.04	1.25	3.31
Il	0.04	2.98	1.01	0.49	0.97	0.51	1.01	1.12	0.40	1.54
Ap	0.14	2.18	0.33	0.14	0.38	0.17	0.19	0.45	0.07	0.57
mg	29.4	43.2	44.4	47.1	53.2	38.1	64.6	38.5	14.0	21.9
	Trace elements in parts per million									
Ba	103	2185	590	70	1182	587	156	1754	278	2441
Li	9	22	17	12	21	7	11	12	4	6
Rb	138	124	88	47	135	34	8	80	98	83
Sr	22	640	162	87	407	232	312	414	57	411
Pb	77	39	18	15	8	3	7	15	22	18
Th	5	8	13	5	9	3	<2	15	16	3
U	<0.5	<0.5	3.5	4.0	1.0	0.5	0.5	1.0	<0.5	<0.5
Zr	56	519	219	175	206	129	134	477	377	916
Nb	<2	48	14	5	9	10	6	38	30	11
Y	23	80	44	16	21	30	24	39	53	19
La	21	177	36	10	25	22	11	104	107	25
Ce	28	350	65	25	48	45	19	175	216	48
Pr	<2	36	8	3	6	5	<2	16	23	6
Nd	7	170	27	12	22	21	12	69	86	24
Sc	3	26	15	4	10	11	23	10	2	18
V	2	110	51	27	51	14	127	42	<2	9
Cr	2	40	15	25	6	2	120	8	1	3
Ni	3	16	12	8	5	3	29	8	3	6
Cu	1	24	13	8	2	2	66	14	1	10
Zn	7	121	49	27	32	45	43	79	59	69
Sn	<2	2	5	2	2	2	3	3	3	<2
Ga	11	25	15	6	16	15	13	19	21	22
As	1.5	2.0	0.5	<0.5	0.5	<0.5	0.5	0.5	4.0	1.0
S	<100	90	100	<100	<100	<100	100	100	20	250

mg = atomic 100 Mg/(Mg + Fe2+)

number of alkaline dykes, sills, and flows whose occurrence has been associated with development of the Lambert rift (e.g., Sheraton & England 1980; Sheraton 1983; Hofmann 1991).

Quartz monzonite ('charnockite') at Loewe Massif

In the northern half of Loewe Massif, a batholith of compositionally varied orthopyroxene-bearing ('charnockitic') granitic rocks intrudes prominently layered felsic orthogneiss and leucogneiss. Occupying an outcrop of 150 km^2, this batholith may be represented by similar rocks at nearby White Massif and Amery Peaks, which would increase its outcrop area to over 300 km^2. Near a sharp, cross-cutting, clearly intrusive contact exposed at the base of the southwest flank of Loewe Massif adjacent to the McKinnon glacier, the batholith contains remnants of assimilated blocks of the leucocratic country rock. Sample 91286407 (lat. 70°35.62′S, long. 67°37′E), from 3 km inside the contact, is a medium to coarse, slightly porphyritic biotite–hornblende–orthopyroxene–quartz monzonite with a hypidiomorphic inequigranular texture cut by microshears. It comprises reddish brown biotite (4%), greenish brown hornblende (4%), orthopyroxene (partly replaced by iddingsite, 4%), quartz (12%), perthite (30%), zoned sodic andesine (45%), and minor ilmenite, magnetite, apatite, and zircon.

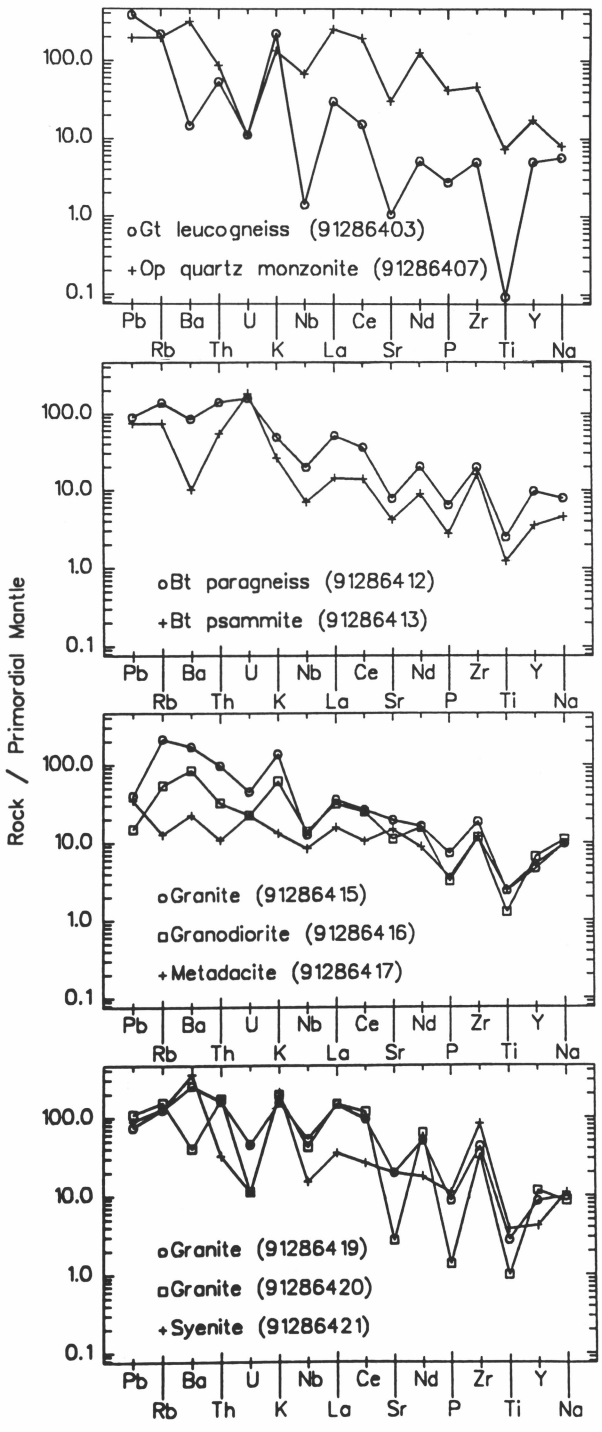

Figure 2. Primordial mantle-normalised incompatible-element-abundance patterns (spidergrams) for the PCM geochronology samples. The normalising values are from Sun & McDonough (1989).

The analysed rock (58.9% SiO_2) belongs to a low-SiO_2 group within the batholith. Its intermediate composition suggests that it originated from a mantle-derived mafic to intermediate magma, possibly through AFC (assimilation–fractional-crystallisation) processes (DePaolo 1981), implying that the rock has a crustal component. Alternatively, it might have originated from the dry partial melting of mafic to intermediate lower-crustal rocks, but this would have required an unusually large heat input. The lack of Y depletion (Fig. 2) precludes both hydrous (and thus lower-temperature) melting with significant residual amphibole, and high-pressure melting with residual garnet. High TiO_2, P_2O_5, Zr, Nb, Y, La, and Ce can be explained by the increased solubilities of minor phases in high-temperature melts (e.g., Watson & Harrison 1983), whether mantle- or crust-derived. Either model would be consistent with the moderate degree of Sr depletion (Fig. 2), implying plagioclase fractionation and/or residual plagioclase during melting. Other samples from the batholith are more siliceous (granite s.s.), and probably represent a distinct magma type formed by the dry melting of lower-crustal granulites (Sheraton et al. 1996).

Zircon grains in the monzonite are up to 600 m long, and have average elongation ratios of 3:1. Most appear to be rounded owing to dominant first-order prismatic faces with multifaceted terminations. Neither optical zoning nor cores are evident. A simple igneous origin befits the zircons, whose terminations were slightly modified later.

Isotopic data for the zircons (Table 2) plotted on a U–Pb concordia diagram (Fig. 3a) largely fall within the limits of analytical uncertainty of a mean $^{207}Pb/^{206}Pb$ age of 980 ± 21 Ma, which is taken as the crystallisation age of the charnockitic quartz monzonite. One discrepant analysis (2.1, shaded in Fig. 3a) has a marginally higher $^{207}Pb/^{206}Pb$ ratio than the mean. The mean $^{206}Pb/^{238}U$ age of the population is 944 ± 41 Ma, which overlaps with the $^{207}Pb/^{206}Pb$ age; the data are concordant to within error. If this analysis is included, the chi-square value (a statistic which compares the population statistics of the unknown with those of the interspersed analyses of the standard) of the entire group is 1.96, and the age 992 ± 28 Ma. For all samples discussed in this paper, the more precise $^{207}Pb/^{206}Pb$ age is preferred.

Leucogneiss at Mount McCarthy

The eastern end of Mount McCarthy is composed of intensely deformed (D_6 L-fabric; Fitzsimons & Thost 1992) garnet-bearing leucogneiss and 'charnockitic' rocks, whose main contact is tectonic. However, at one locality several sheets and irregular pods of leucogneiss clearly intrude the 'charnockitic' rock (Fitzsimons & Thost 1992, fig. 3d). Sample 91286403 (lat. 70°24.25′S, long. 66°36′E), from the largest of these intrusive leucogneiss bodies, is an inequigranular garnet leucogranite–gneiss consisting of ribbon quartz, sericitised perthite and subordinate sericitised plagioclase, together with garnet (1%) and minor muscovite and zircon. The rock is markedly

peraluminous (ASI 1.10), although not to the extent that an S-type origin is certain. It probably resulted from the local partial melting of either metasedimentary or a mixture of metasedimentary and meta-igneous country rocks when they were intruded by the 'charnockitic' magma. It is intensely fractionated (low TiO_2, MgO, CaO, Ba, Sr, Zr, Nb, La, Ce, V, Cr, and Ni), and has a highly irregular spidergram with a large negative Sr anomaly (Fig. 2), typical of partial melts of plagioclase-rich felsic crustal rocks (Tarney et al. 1987).

Zircon in the leucogneiss forms mostly elongate grains up to 450 μm long with length:breadth ratios as much as 6:1. Other grains are more equant. Many have overgrowths and distinct cores. Although the cores are mostly anhedral, some are internally zoned and have inclusions, imparting an igneous appearance. The overgrowths, in contrast, are mostly irregular in shape, unzoned, devoid of inclusions, and less clearly of igneous origin.

Twenty-four zircon grains from this sample were analysed. Among two old, ca 1850-Ma cores (15.2 and 27.1), one is enclosed by a ca 1650-Ma overgrowth (15.1, discordant analysis). The remaining analyses gave a mean $^{207}Pb/^{206}Pb$ age of 997 ± 21 Ma. However, the chi-square value of 4.3 for this group indicates more scatter in the data than for a single age population. Some of the scatter might be the result of Pb loss associated with the high U contents (>800 ppm) of some grains, but the behaviour is non-systematic. Even separating the data for core and rim populations (Figs. 3b, c) does not eliminate the scatter: the rims (3.1, 6.1, 7.2, 10.2, 13.1, 17.1, and 25.2) yield a mean $^{207}Pb/^{206}Pb$ age of 994 ± 39 Ma and a chi-square value of 5.4, and the cores (3.2, 6.2, 7.1, 10.1, 13.2, and 25.1) 1005 ± 57 Ma and 3.9. The chi-square value of the cores can be reduced to unity by deleting analysis 13.2 (perhaps a slightly older core), resulting in a revised age of 990 ± 30 Ma, but the ages yielded by the two morphological subgroups remain indistinguishable. There are several possible interpretations: the cores might be inherited from the source while the rims formed during the melting; both cores and rims might have formed during the same melting event; or the cores might have formed during the melting, and the rims were added later. Regardless, the bulk of the isotopic data suggest that partial melting to form the leucogneiss occurred about 990 Ma ago.

Granite and volcanics at Fisher Massif

Fisher Massif (300 km^2) is composed of thick-layered meta-volcanic, pyroclastic, and minor metasedimentary rocks, and intrusive igneous rocks ranging in composition from gabbro to granite (Fedorov et al. 1987; Crowe 1994; Kamenev et al. 1993; Mikhalsky et al. 1996). The metavolcanics, mainly mafic, include amygdaloidal basalt and ultramafic and intermediate to felsic varieties. Associated metasediments include banded ironstone, calcarenite, and conglomerate with clasts of siliceous rock and ironstone in a sandy matrix. Mineral assemblages in these rocks reflect lower-amphibolite-facies metamorphism with estimated P–T peaks of 0.1–0.3 GPa and 450–550°C, and subsequent retrogression to the greenschist facies (Crowe 1994). The volcanics have an early steeply dipping S1 fabric folded into tight F2 structures and later broken up by mylonitic faults. Granodioritic intrusions are cut by undeformed but metamorphosed mafic dykes which do not appear to cut a later granite in the north. One sample of each from the granite, granodiorite, and felsic volcanics were selected for study.

Sample 91286415 (lat. 71°26.73′S, long. 67°51′E) is an undeformed medium-grained biotite granite from Blustery Cliffs, at the northeast end of Fisher Massif. The sharply intrusive but locally sheared contact between this granite and mafic volcanic country rocks is exposed on the side of an

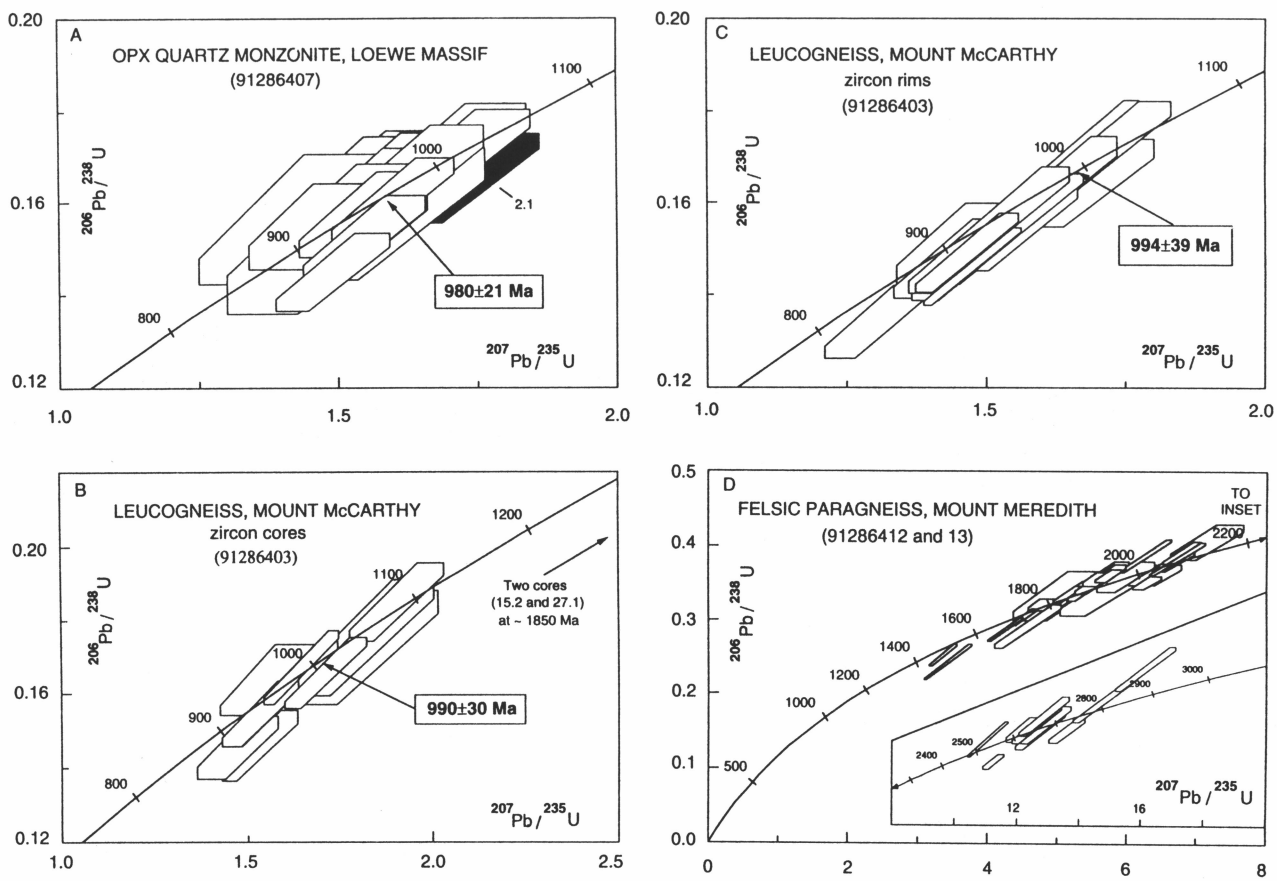

Figure 3. U–Pb concordia diagrams showing SHRIMP data for samples from the Loewe Massif, Mount McCarthy, and Mount Meredith. Error boxes reflect 95% confidence limits.

Table 2. U–Th–Pb isotopic compositions of zircons from the northern Prince Charles Mountains.

Grain area	*U (μg/g)*	*Th (μg/g)*	*Th/U*	$^{206}Pb/^{204}Pb$	f_{206} %	$^{206}Pb/^{238}U$ *±1σ error*	$^{207}Pb/^{235}U$ *±1σ error*	$^{207}Pb/^{206}Pb$ *±1σ error*	$^{207}Pb/^{206}Pb$ *Age (Ma)±1σ*	*% conc*
					91286407 (orthopyroxene–quartz monzonite, Loewe Massif)					
1.1	299	173	0.580	4471	0.382	0.1457±0.0069	1.398±0.078	0.0696±0.0017	917±51	96
2.1	209	273	1.309	53100	0.032	0.1515±0.0072	1.595±0.082	0.0764±0.0012	1105±31	82
4.1	164	231	1.407	110000	0.016	0.1398±0.0066	1.419±0.074	0.0736±0.0012	1031±33	82
5.1	145	180	1.246	37600	0.045	0.1504±0.0071	1.530±0.083	0.0738±0.0016	1036±44	87
8.1	405	433	1.070	15500	0.110	0.1591±0.0075	1.587±0.081	0.0723±0.0011	996±31	96
9.1	291	333	1.145	5070	0.337	0.1704±0.0080	1.695±0.092	0.0721±0.0016	990±44	102
11.1	182	101	0.557	7307	0.234	0.1596±0.0075	1.579±0.091	0.0717±0.0020	979±57	98
12.1	233	236	1.011	8157	0.209	0.1468±0.0069	1.431±0.080	0.0707±0.0018	949±52	93
14.1	154	123	0.798	2025	0.843	0.1537±0.0073	1.489±0.099	0.0703±0.0029	936±87	98
16.1	375	171	0.455	13100	0.130	0.1562±0.0074	1.532±0.081	0.0711±0.0014	961±40	97
19.1	193	279	1.441	6492	0.263	0.1481±0.0070	1.435±0.081	0.0703±0.0018	936±54	95
20.1	406	551	1.359	16300	0.105	0.1439±0.0068	1.479±0.076	0.0746±0.0011	1057±31	82
22.1	177	135	0.761	1607	1.062	0.1576±0.0074	1.482±0.098	0.0682±0.0028	874±87	108
24.1	151	151	1.004	4810	0.355	0.1647±0.0078	1.579±0.092	0.0695±0.0020	914±60	108
26.1	226	272	1.205	23700	0.072	0.1692±0.0080	1.705±0.091	0.0731±0.0014	1017±40	99
29.1	242	186	0.766	4701	0.363	0.1744±0.0082	1.715±0.093	0.0713±0.0015	966±43	107
30.1	172	112	0.647	6272	0.272	0.1727±0.0082	1.696±0.101	0.0712±0.0022	964±65	106
33.1	189	189	1.000	3617	0.472	0.1719±0.0081	1.624±0.096	0.0685±0.0021	884±64	116
34.1	157	99	0.632	2291	0.745	0.1680±0.0079	1.531±0.096	0.0661±0.0024	809±77	124
37.1	191	121	0.632	12500	0.137	0.1606±0.0076	1.566±0.088	0.0707±0.0018	950±53	101
38.1	177	191	1.080	10500	0.162	0.1692±0.0080	1.686±0.108	0.0723±0.0027	994±78	101
					91286403 (garnet leucogneiss, Mount McCarthy)					
3.1	2010	73	0.036	8402	0.203	0.1579±0.0074	1.534±0.074	0.0704±0.0004	941±13	100
3.2	1120	79	0.070	47100	0.036	0.1533±0.0072	1.510±0.073	0.0714±0.0005	970±14	95
6.1	634	233	0.367	10900	0.157	0.1531±0.0072	1.552±0.077	0.0736±0.0007	1029±21	89
6.2	116	93	0.803	7142	0.239	0.1626±0.0077	1.591±0.100	0.0709±0.0025	956±75	102
7.1	598	264	0.442	8198	0.208	0.1533±0.0072	1.522±0.077	0.0720±0.0009	987±27	93
7.2	1839	155	0.084	1731	0.986	0.1629±0.0077	1.667±0.088	0.0742±0.0014	1048±37	93
10.1	858	284	0.331	8438	0.202	0.1837±0.0087	1.889±0.096	0.0746±0.0010	1058±27	103
10.2	2795	236	0.085	96600	0.018	0.1449±0.0068	1.464±0.070	0.0733±0.0003	1022±8	85
13.1	884	150	0.169	1887	0.904	0.1498±0.0071	1.451±0.083	0.0703±0.0019	936±57	96
13.2	700	324	0.462	7804	0.219	0.1449±0.0068	1.520±0.077	0.0761±0.0010	1098±26	79
15.1	1282	40	0.031	42100	0.038	0.2506±0.0118	3.501±0.169	0.1013±0.0006	1648±12	87
15.2	801	104	0.130	390000	0.004	0.3018±0.0142	4.661±0.223	0.1120±0.0005	1832±8	93
17.1	939	129	0.138	11300	0.151	0.1330±0.0063	1.291±0.067	0.0704±0.0011	940±32	86
18.1	569	115	0.201	8257	0.207	0.1707±0.0080	1.706±0.086	0.0725±0.0009	999±25	102
21.1	711	151	0.213	11500	0.149	0.1467±0.0069	1.416±0.070	0.0700±0.0008	928±23	95
23.1	569	469	0.825	15300	0.112	0.1644±0.0077	1.698±0.084	0.0749±0.0008	1066±21	92
25.1	377	205	0.544	32600	0.052	0.1443±0.0068	1.461±0.077	0.0734±0.0014	1026±39	85

Table 2. cont.

Grain area	*U (µg/g)*	*Th (µg/g)*	*Th/U*	$^{206}Pb/^{204}Pb$	f_{206} %	$^{206}Pb/^{238}U$ *±1σ error*	$^{207}Pb/^{235}U$ *±1σ error*	$^{207}Pb/^{206}Pb$ *±1σ error*	$^{207}Pb/^{206}Pb$ *Age (Ma)±1σ*	*% conc*
25.2	1027	102	0.100	270000	0.006	0.1478±0.0069	1.454±0.071	0.0714±0.0006	967±18	92
27.1	863	159	0.184	55600	0.028	0.3430±0.0161	5.378±0.257	0.1137±0.0005	1859±7	102
28.1	150	146	0.969	22600	0.075	0.1856±0.0088	1.950±0.112	0.0762±0.0021	1100±56	100
31.1	670	153	0.228	4355	0.392	0.1719±0.0081	1.710±0.086	0.0722±0.0009	990±26	103
32.1	445	153	0.343	3331	0.512	0.1638±0.0077	1.634±0.086	0.0723±0.0013	995±37	98
35.1	262	182	0.695	4185	0.408	0.1885±0.0089	1.951±0.106	0.0751±0.0016	1070±43	104
36.1	486	108	0.222	13000	0.132	0.1654±0.0078	1.618±0.081	0.0709±0.0009	955±26	103
					91286415 (biotite granite, Fisher Massif)					
18.1	129	79	0.609	1101	1.533	0.1772±0.0054	1.693±0.135	0.0693±0.0048	907±151	116
19.1	108	81	0.750	1913	0.883	0.1717±0.0052	1.783±0.122	0.0753±0.0044	1077±121	95
22.1	111	66	0.592	1923	0.878	0.1818±0.0054	1.853±0.113	0.0739±0.0037	1040±103	104
23.1	138	103	0.742	2757	0.612	0.1796±0.0053	1.857±0.086	0.0750±0.0024	1067±65	100
26.1	223	227	1.021	2992	0.564	0.1769±0.0052	1.843±0.080	0.0756±0.0021	1083±58	97
27.1	74	58	0.777	500	3.376	0.1697±0.0053	1.396±0.179	0.0597±0.0072	591±286	171
30.1	63	47	0.749	536	3.152	0.1782±0.0056	1.494±0.231	0.0608±0.0090	632±354	167
31.1	143	128	0.896	1963	0.860	0.1868±0.0056	1.908±0.107	0.0741±0.0032	1044±91	106
34.1	100	70	0.700	1455	1.160	0.1790±0.0054	1.726±0.106	0.0699±0.0035	926±107	115
35.1	72	45	0.626	805	2.097	0.1796±0.0055	1.727±0.148	0.0698±0.0053	921±166	116
38.1	134	90	0.670	2550	0.662	0.1832±0.0054	1.935±0.105	0.0766±0.0032	1111±86	98
39.1	166	101	0.608	4170	0.405	0.1865±0.0055	1.856±0.075	0.0722±0.0017	991±49	111
42.1	104	65	0.620	1250	1.350	0.1791±0.0054	1.721±0.126	0.0697±0.0044	920±135	115
43.1	135	117	0.866	979	1.724	0.1564±0.0047	1.591±0.115	0.0738±0.0046	1036±132	90
46.1	153	99	0.642	1891	0.893	0.1848±0.0055	1.907±0.109	0.0748±0.0034	1064±94	103
47.1	81	54	0.660	1211	1.539	0.1888±0.0057	1.868±0.139	0.0717±0.0046	979±137	114
					91286416 (biotite ± hornblende granodiorite, Fisher Massif)					
20.1	113	82	0.725	5072	0.325	0.2231±0.0067	2.580±0.134	0.0839±0.0033	1290±8	101
21.1	106	59	0.553	4694	0.352	0.2245±0.0067	2.613±0.113	0.0844±0.0024	1302±55	100
24.1	210	192	0.916	40300	0.041	0.2208±0.0065	2.649±0.101	0.0870±0.0018	1361±41	95
25.1	107	55	0.513	1854	0.890	0.2220±0.0067	2.527±0.143	0.0826±0.0037	1259±90	103
28.1	132	138	1.044	2742	0.602	0.2122±0.0063	2.417±0.109	0.0826±0.0025	1260±61	98
29.1	172	80	0.466	5159	0.320	0.2219±0.0066	2.613±0.107	0.0854±0.0021	1325±49	97
32.1	61	23	0.376	851	1.939	0.2200±0.0068	2.221±0.199	0.0732±0.0059	1020±172	126
33.1	106	58	0.541	10500	0.158	0.2309±0.0069	2.747±0.124	0.0863±0.0026	1345±60	100
36.1	100	65	0.648	11700	0.141	0.2254±0.0069	2.645±0.219	0.0851±0.0062	1318±149	99
37.1	330	336	1.019	18900	0.087	0.2221±0.0065	2.581±0.086	0.0843±0.0011	1299±25	100
40.1	108	55	0.505	2583	0.639	0.2278±0.0068	2.613±0.126	0.0832±0.0029	1274±69	104
41.1	134	99	0.735	3510	0.470	0.2313±0.0069	2.729±0.111	0.0856±0.0021	1329±47	101
44.1	91	56	0.614	10800	0.152	0.2252±0.0068	2.678±0.133	0.0862±0.0031	1343±71	97
45.1	87	49	0.563	1161	1.421	0.2346±0.0071	2.337±0.146	0.0722±0.0037	993±107	137

Table 2. cont.

Grain area	*U (μg/g)*	*Th (μg/g)*	*Th/U*	$^{206}Pb/^{204}Pb$	f_{206} %	$^{206}Pb/^{238}U$ *±1σ error*	$^{207}Pb/^{235}U$ *±1σ error*	$^{207}Pb/^{206}Pb$ *±1σ error*	$^{207}Pb/^{206}Pb$ *Age (Ma)±1σ*	% *conc*
48.1	96	58	0.604	2420	0.682	0.2328±0.0070	2.673±0.137	0.0833±0.0032	1276±76	106
49.1	165	120	0.725	2400	0.688	0.2298±0.0068	2.589±0.112	0.0817±0.0023	1238±56	108
50.1	85	33	0.394	1916	0.861	0.2262±0.0068	2.507±0.134	0.0804±0.0033	1206±82	109
						91286417 (metadacite, Fisher Massif)				
2.1	316	383	1.213	9571	0.173	0.2249±0.0048	2.704±0.066	0.0872±0.0008	1365±18	96
3.1	141	113	0.799	4331	0.381	0.2272±0.0049	2.644±0.076	0.0844±0.0014	1302±33	101
4.1	119	82	0.686	1000000	0.002	0.1808±0.0039	1.975±0.051	0.0792±0.0009	1178±23	91
5.1	87	59	0.680	1194	1.384	0.2065±0.0046	2.163±0.123	0.0760±0.0038	1094±103	111
6.1	126	106	0.844	4749	0.348	0.2193±0.0048	2.474±0.082	0.0818±0.0018	1241±45	103
5.2	143	116	0.810	2975	0.555	0.2139±0.0046	2.436±0.085	0.0826±0.0021	1260±50	99
6.2	160	151	0.940	3220	0.513	0.2186±0.0047	2.510±0.079	0.0833±0.0017	1276±40	100
7.1	136	107	0.783	4226	0.391	0.2112±0.0046	2.391±0.079	0.0821±0.0018	1248±45	99
8.1	645	871	1.351	3972	0.416	0.2203±0.0047	2.531±0.061	0.0833±0.0008	1277±19	100
9.1	139	112	0.804	3768	0.439	0.2233±0.0048	2.558±0.079	0.0831±0.0016	1271±38	102
10.1	77	58	0.749	5257	0.314	0.2246±0.0050	2.592±0.105	0.0837±0.0026	1286±62	102
2.2	205	190	0.929	4168	0.396	0.2301±0.0049	2.685±0.081	0.0846±0.0016	1307±37	102
11.1	80	68	0.849	1000000	0.002	0.1805±0.0039	1.875±0.053	0.0753±0.0012	1077±32	99
12.1	185	99	0.535	1486	1.112	0.1607±0.0034	1.667±0.068	0.0752±0.0024	1074±66	89
13.1	693	1047	1.512	2744	0.602	0.2242±0.0047	2.506±0.061	0.0811±0.0008	1223±20	107
14.1	148	83	0.563	3357	0.492	0.2121±0.0046	2.548±0.083	0.0871±0.0019	1363±43	91
15.1	336	153	0.455	11400	0.145	0.3393±0.0072	5.515±0.125	0.1179±0.0007	1924±10	98
16.1	380	457	1.204	4444	0.372	0.2251±0.0048	2.615±0.066	0.0842±0.0010	1298±22	101
17.1	91	61	0.674	1016	1.625	0.2319±0.0051	2.351±0.127	0.0735±0.0034	1029±97	131
8.2	652	908	1.392	2020	0.818	0.2234±0.0047	2.468±0.065	0.0801±0.0011	1200±27	108
						91286419 (grey granite, Mount Collins)				
1.1	21	12	0.600	4470	0.382	0.1663±0.0045	1.868±0.266	0.0815±0.0111	1232±294	80
2.1	135	67	0.497	4060	0.420	0.1623±0.0034	1.534±0.070	0.0686±0.0026	886±80	109
3.1	331	254	0.768	56800	0.030	0.1656±0.0034	1.684±0.047	0.0738±0.0013	1035±35	95
4.1	141	99	0.702	1828	0.934	0.1613±0.0034	1.459±0.075	0.0656±0.0029	793±95	122
5.1	111	66	0.593	19900	0.086	0.1647±0.0035	1.650±0.066	0.0726±0.0023	1004±65	98
6.1	63	42	0.660	11800	0.145	0.1759±0.0039	1.762±0.109	0.0726±0.0040	1004±116	104
6.2	113	52	0.458	2152	0.793	0.1608±0.0034	1.510±0.080	0.0681±0.0031	871±98	110
8.1	45	23	0.504	1117	1.527	0.1664±0.0039	1.480±0.159	0.0645±0.0066	758±230	131
9.1	46	24	0.531	1473	1.158	0.1764±0.0041	1.602±0.157	0.0659±0.0061	803±207	130
11.1	183	81	0.445	3471	0.492	0.1649±0.0034	1.576±0.058	0.0693±0.0019	908±59	108
12.1	441	189	0.429	50300	0.034	0.1662±0.0034	1.685±0.041	0.0735±0.0008	1028±22	96
13.1	47	22	0.464	1721	0.991	0.1582±0.0036	1.536±0.142	0.0704±0.0061	939±189	101
14.1	883	455	0.515	43600	0.039	0.1781±0.0036	1.743±0.039	0.0710±0.0006	957±16	110

Table 2. cont.

Grain area	*U (μg/g)*	*Th (μg/g)*	*Th/U*	$^{206}Pb/^{204}Pb$	f_{206} %	$^{206}Pb/^{238}U$ *±1σ error*	$^{207}Pb/^{235}U$ *±1σ error*	$^{207}Pb/^{206}Pb$ *±1σ error*	$^{207}Pb/^{206}Pb$ *Age (Ma)±1σ*	*% conc*
					91286420 (pink granite, Mount Collins)					
3.1	449	209	0.466	220000	0.008	0.1673±0.0032	1.679±0.035	0.0728±0.0005	1009±15	99
4.1	405	160	0.394	9925	0.172	0.1578±0.0030	1.533±0.036	0.0705±0.0008	942±24	100
7.1	319	195	0.609	37900	0.045	0.1639±0.0031	1.618±0.037	0.0716±0.0008	974±22	100
8.1	623	338	0.542	130000	0.014	0.1578±0.0030	1.572±0.033	0.0723±0.0005	994±15	95
11.1	460	137	0.297	92400	0.018	0.1584±0.0030	1.597±0.035	0.0731±0.0006	1017±18	93
12.1	394	78	0.197	140000	0.012	0.1584±0.0030	1.584±0.034	0.0725±0.0006	1000±17	95
16.1	1223	585	0.478	3000000	0.001	0.1684±0.0031	1.670±0.033	0.0719±0.0003	984±9	102
17.1	680	443	0.651	150000	0.012	0.1667±0.0031	1.645±0.034	0.0716±0.0005	973±14	102
20.1	682	322	0.472	156000	0.011	0.1679±0.0031	1.665±0.034	0.0719±0.0004	984±12	102
21.1	422	155	0.368	13300	0.128	0.1668±0.0031	1.637±0.038	0.0712±0.0008	963±23	103
24.1	318	41	0.130	61700	0.028	0.1728±0.0033	1.702±0.038	0.0714±0.0007	970±19	106
25.1	379	152	0.402	13900	0.123	0.1665±0.0031	1.617±0.040	0.0704±0.0010	940±28	106
28.1	490	134	0.273	13100	0.130	0.1639±0.0031	1.618±0.036	0.0716±0.0007	974±21	100
29.1	583	427	0.733	27500	0.062	0.1604±0.0030	1.582±0.035	0.0715±0.0007	972±19	99
32.1	501	206	0.412	72900	0.023	0.1621±0.0031	1.629±0.037	0.0729±0.0007	1011±21	96
34.1	493	197	0.400	82100	0.021	0.1641±0.0031	1.632±0.035	0.0721±0.0006	990±17	99
35.1	444	177	0.398	18000	0.095	0.1674±0.0032	1.629±0.040	0.0706±0.0010	946±28	105
38.1	343	122	0.356	16600	0.103	0.1664±0.0032	1.630±0.040	0.0711±0.0010	959±28	103
39.1	501	264	0.526	24700	0.069	0.1720±0.0033	1.690±0.040	0.0713±0.0008	965±24	106
42.1	370	403	1.092	23000	0.074	0.1645±0.0031	1.644±0.044	0.0725±0.0012	999±33	98
43.1	303	274	0.904	8011	0.213	0.1640±0.0032	1.610±0.043	0.0712±0.0012	964±34	102
44.1	438	181	0.415	22000	0.077	0.1708±0.0033	1.684±0.040	0.0715±0.0009	971±24	105
45.1	462	203	0.440	17000	0.100	0.1679±0.0032	1.651±0.037	0.0713±0.0007	966±21	104
48.1	451	219	0.485	27400	0.062	0.1612±0.0030	1.612±0.036	0.0725±0.0007	1001±20	96
49.1	595	63	0.105	850000	0.002	0.1516±0.0028	1.514±0.032	0.072±0.0005	998±15	91
52.1	555	170	0.307	38600	0.044	0.1674±0.0031	1.669±0.036	0.0723±0.0006	994±18	100
53.1	421	211	0.501	100000	0.017	0.1628±0.0031	1.605±0.035	0.0715±0.0006	972±18	100
					91286421 (pyroxene–quartz syenite, Mount Collins)					
1.1	108	31	0.290	5247	0.325	0.1679±0.0034	1.628±0.066	0.0703±0.0023	938±70	107
2.1	153	118	0.770	15000	0.114	0.1635±0.0032	1.596±0.047	0.0708±0.0014	951±42	103
5.1	229	124	0.543	17100	0.100	0.1601±0.0030	1.620±0.042	0.0734±0.0011	1025±32	93
6.1	205	152	0.741	6211	0.275	0.1595±0.0031	1.551±0.045	0.0706±0.0014	944±41	101
9.1	155	45	0.289	3968	0.430	0.1725±0.0034	1.636±0.058	0.0688±0.0019	893±58	115
10.1	148	90	0.606	29400	0.058	0.1554±0.0030	1.560±0.047	0.0728±0.0015	1009±42	92
13.1	103	48	0.461	24300	0.070	0.1643±0.0032	1.623±0.054	0.0716±0.0017	976±50	100
14.1	224	105	0.471	51400	0.033	0.1648±0.0031	1.649±0.042	0.0726±0.0011	1002±30	98
18.1	349	163	0.467	550000	0.003	0.1667±0.0032	1.674±0.036	0.0728±0.0006	1009±16	99
19.1	713	517	0.724	24200	0.071	0.1667±0.0031	1.657±0.035	0.0720±0.0005	987±15	101

Table 2. cont.

Grain area	*U (μg/g)*	*Th (μg/g)*	*Th/U*	$^{206}Pb/^{204}Pb$	f_{206} %	$^{206}Pb/^{238}U$ ±1σ *error*	$^{207}Pb/^{235}U$ ±1σ *error*	$^{207}Pb/^{206}Pb$ ±1σ *error*	$^{207}Pb/^{206}Pb$ *Age (Ma)*±1σ	% *conc*
22.1	93	38	0.405	30500	0.056	0.1690±0.0033	1.654±0.058	0.0710±0.0019	958±55	105
23.1	131	62	0.472	78500	0.022	0.1651±0.0032	1.699±0.043	0.0746±0.0010	1058±28	93
26.1	160	71	0.443	1627	1.049	0.1653±0.0032	1.616±0.063	0.0709±0.0023	954±66	103
27.1	251	144	0.573	56900	0.030	0.1644±0.0031	1.643±0.040	0.0725±0.0010	999±27	98
30.1	140	84	0.600	10300	0.166	0.1706±0.0033	1.690±0.053	0.0718±0.0016	981±46	103
31.1	269	153	0.571	14200	0.120	0.1708±0.0033	1.661±0.041	0.0705±0.0010	944±29	108
33.1	167	123	0.735	20900	0.082	0.1586±0.0031	1.602±0.057	0.0732±0.0020	1021±56	93
36.1	259	149	0.576	45100	0.038	0.1560±0.0030	1.554±0.045	0.0723±0.0014	993±41	94
37.1	91	43	0.473	44300	0.039	0.1682±0.0034	1.658±0.053	0.0715±0.0016	971±46	103
40.1	180	115	0.637	15500	0.110	0.1672±0.0033	1.640±0.047	0.0712±0.0014	962±39	104
41.1	329	184	0.559	32800	0.052	0.1666±0.0032	1.627±0.039	0.0708±0.0009	952±26	104
19.2	246	141	0.576	14200	0.121	0.1594±0.0030	1.559±0.042	0.0709±0.0012	955±35	100
33.2	223	163	0.731	2762	0.618	0.1678±0.0033	1.569±0.060	0.0678±0.0021	862±65	116
46.1	188	65	0.345	8648	0.197	0.1629±0.0031	1.635±0.048	0.0728±0.0014	1009±40	96
47.1	160	64	0.399	5640	0.303	0.1654±0.0032	1.643±0.056	0.0721±0.0018	988±53	100
50.1	217	89	0.413	11300	0.151	0.1681±0.0033	1.636±0.043	0.0706±0.0011	946±32	106
51.1	128	46	0.358	23100	0.074	0.1621±0.0032	1.595±0.054	0.0714±0.0018	968±53	100
54.1	191	102	0.534	37500	0.046	0.1653±0.0032	1.644±0.042	0.0721±0.0011	989±30	100
55.1	283	178	0.631	21600	0.079	0.1619±0.0031	1.612±0.044	0.0722±0.0012	991±35	98
						91286413 (felsic layer, paragneiss, Mount Meredith)				
1.1	500	175	0.350	3281	0.458	0.3923±0.0074	6.792±0.138	0.1256±0.0007	2037±10	105
2.1	458	274	0.599	2513	0.597	0.3910±0.0074	6.801±0.140	0.1262±0.0008	2045±12	104
4.1	100	40	0.400	806	1.719	0.5090±0.0100	12.294±0.308	0.1752±0.0023	2608±22	102
5.1	238	178	0.749	1444	1.054	0.3667±0.0070	5.753±0.135	0.1138±0.0013	1861±21	108
5.2	379	320	0.844	1984	0.767	0.3622±0.0068	5.712±0.124	0.1144±0.0010	1870±16	107
7.1	141	90	0.634	4303	0.313	0.5081±0.0098	13.641±0.293	0.1947±0.0015	2782±12	95
9.1	74	47	0.636	1355	1.108	0.3623±0.0072	6.406±0.191	0.1282±0.0026	2074±36	96
10.1	414	142	0.342	12400	0.126	0.3351±0.0063	5.145±0.107	0.1113±0.0007	1821±12	102
10.2	566	160	0.283	5909	0.264	0.3043±0.0057	4.529±0.092	0.1079±0.0006	1765±11	97
12.1	340	228	0.671	3688	0.417	0.3393±0.0064	5.378±0.114	0.1150±0.0009	1879±14	100
13.1	235	132	0.559	2365	0.635	0.3806±0.0072	6.674±0.148	0.1272±0.0012	2059±16	101
14.1	149	86	0.578	3227	0.426	0.5305±0.0156	12.901±0.399	0.1764±0.0012	2619±11	105
15.1	146	89	0.610	2106	0.653	0.5177±0.0152	12.668±0.394	0.1775±0.0013	2629±12	102
16.1	89	28	0.315	783	1.890	0.4066±0.0120	7.150±0.265	0.1276±0.0024	2065±34	107
16.2	1028	5	0.005	6521	0.244	0.2526±0.0073	3.358±0.101	0.0964±0.0005	1556±9	93
17.1	714	478	0.669	8953	0.157	0.4942±0.0144	11.099±0.328	0.1629±0.0004	2486±5	104
18.1	270	133	0.493	1827	0.839	0.3561±0.0104	5.624±0.181	0.1146±0.0012	1873±19	105
20.1	628	251	0.399	11200	0.132	0.3833±0.0111	6.724±0.200	0.1272±0.0005	2060±7	102
24.1	233	126	0.539	2558	0.526	0.5531±0.0162	14.737±0.448	0.1932±0.0010	2770±9	102
24.2	1292	6	0.005	10800	0.145	0.2878±0.0083	4.256±0.126	0.1073±0.0004	1753±6	93

Table 2. cont.

Grain area	*U (μg/g)*	*Th (μg/g)*	*Th/U*	$^{206}Pb/^{204}Pb$	f_{206} %	$^{206}Pb/^{238}U$ *±1σ error*	$^{207}Pb/^{235}U$ *±1σ error*	$^{207}Pb/^{206}Pb$ *±1σ error*	$^{207}Pb/^{206}Pb$ *Age (Ma)±1σ*	*% conc*
25.1	139	38	0.273	1878	0.732	0.5171±0.0152	12.956±0.407	0.1817±0.0014	2669±13	101
26.1	116	43	0.374	2679	0.511	0.5075±0.0150	12.795±0.403	0.1829±0.0014	2679±13	99
27.1	122	65	0.536	1630	0.932	0.3597±0.0106	5.988±0.210	0.1207±0.0019	1967±28	101
28.2	1049	321	0.306	4789	0.316	0.3879±0.0113	6.272±0.187	0.1173±0.0005	1915±8	110
29.1	298	103	0.344	5499	0.246	0.6081±0.0178	16.155±0.488	0.1927±0.0009	2765±8	111
30.1	86	72	0.835	964	1.525	0.3410±0.0172	5.716±0.337	0.1216±0.0030	1979±45	96
30.2	1536	14	0.009	5259	0.299	0.2433±0.0122	3.423±0.174	0.1020±0.0004	1662±8	84
						91286412 (paragneiss, Mount Meredith)				
32.1	81	37	0.464	577	2.586	0.3334±0.0169	5.034±0.326	0.1095±0.0038	1792±64	104
32.2	353	49	0.139	1922	0.787	0.2920±0.0146	4.582±0.242	0.1138±0.0013	1861±21	89
33.1	284	134	0.474	6750	0.229	0.3457±0.0044	5.350±0.092	0.1122±0.0011	1836±18	104
34.1	257	149	0.580	5103	0.292	0.3514±0.0045	6.292±0.103	0.1299±0.0012	2096±16	93
35.1	260	67	0.257	7101	0.194	0.4586±0.0058	11.277±0.167	0.1784±0.0011	2638±10	92
37.1	205	105	0.512	13900	0.110	0.3609±0.0046	5.740±0.096	0.1153±0.0011	1885±17	105
38.1	156	82	0.524	3987	0.387	0.3558±0.0047	5.579±0.110	0.1137±0.0015	1859±24	106
40.1	109	76	0.693	1368	1.135	0.3212±0.0043	4.868±0.138	0.1099+0.0026	1798±43	100

f_{206} is the proportion, expressed as a percentage, of common ^{206}Pb to total ^{206}Pb. The reported ages are derived from radiogenic $^{207}Pb/^{206}Pb$ ratios. % conc is the relative concordance of the isotopic ages; values less than 100% plot below concordia, and values above 100% plot above concordia. The grain area values represent sequentional analytical order. Gaps in the order do not indicate that data have been omitted; some reflect the abortion of a partial analysis owing to technical considerations, whereas others are due to the intermingling of analyses from different samples (as for samples 91286403 and 91286407).

arête between two alpine glaciers. At this locality the somewhat altered granite contains abundant mafic xenoliths, biotite aggregates (~4%) which might be partly of secondary origin, and sericitised oligoclase. Accessory minerals are allanite, titanite, zircon, apatite, and magnetite, plus secondary muscovite, chlorite, carbonate, and ?prehnite. Offshoots of the granite cut the volcanics.

Sample 91286416 (lat. 71°28.75′S, long. 67°45′E) was collected from a medium-grained, foliated biotite ± hornblende granodiorite in the central part of Fisher Massif. A major mylonite zone forms the boundary between the granodiorite and volcanics here, whereas other contacts are poorly exposed (moraine-covered). Unlike the biotite granite, the granodiorite is cut by numerous undeformed mafic dykes, suggesting that it is the older of the two intrusions. Its texture is hypidiomorphic inequigranular, but the rock is considerably recrystallised and altered; plagioclase (zoned oligoclase), in particular, is sericitised, and near the mylonite zone the granodiorite is highly sheared. Dark brown biotite (5%) occurs both as large grains and fine-grained aggregates. Minor phases are allanite, titanite, zircon, apatite, ilmenite, magnetite, epidote, muscovite, chlorite, and carbonate. Hornblende is absent from the sample, but occurs in other parts of the granodiorite.

Neither of the Fisher Massif intrusives clearly represents juvenile felsic crust, because Ce/Y ratios — and, by implication, rare-earth-element (REE) fractionation — are too low to be consistent with the melting of a garnet-bearing mafic source in the mantle; however, an amphibolite source (e.g., subducted, hydrated oceanic crust) could have produced the melt from which these intrusives were derived. Both samples have irregular spidergrams (depleted in P and Ti relative to light REE and Zr) typical of intracrustal melts, yet neither shows the marked Sr depletion consistent with major plagioclase control (Fig. 2). The moderately high Y (30 ppm), low Ce/Y_n (3.8, chondrite-normalised), and Sr depletion of the granodiorite (91286416) indicate that either residual plagioclase or plagioclase fractionation, or both, were of some significance, and that an intracrustal origin is more likely for this sample than for 91286415. The younger granite (91286415) — with 21 ppm Y, Ce/Y_n of 5.7, and, more significantly, little or no Sr depletion — may represent new crust, although isotopic data would be necessary to confirm this. Melting of intermediate to felsic lower-crustal rocks cannot be discounted, but the lack of an Sr anomaly requires very high degrees of melting (Champion & Sheraton 1993).

Zircon grains in sample 91286415 are moderately uniform, averaging about 180 × 90 μm. They are euhedral to subhedral, clear and unzoned, and evidently of igneous origin. Perfectly preserved terminations composed of both primary and secondary pyramids are common, as are primary and secondary prisms. All 16 analyses define a statistically simple concordant population with $^{206}Pb/^{238}U$, $^{207}Pb/^{235}U$, and $^{207}Pb/^{206}Pb$ ages of 1056 ± 24, 1048 ± 25, and 1020 ± 48 Ma respectively (Fig. 4a). The last is preferred as the crystallisation age of the granite.

The slightly larger zircons in 91286416 (averaging 220 × 90 μm) are mostly subhedral, not visibly zoned, and cloudy, presumably because they contain tiny inclusions. However, they include some clear grains, and others with a faint zoning. Both primary and secondary prisms and pyramids are common. All 17 analyses form a statistically simple concordant population with $^{206}Pb/^{238}U$, $^{207}Pb/^{235}U$, and $^{207}Pb/^{206}Pb$ ages of 1309 ± 29, 1297 ± 23, and 1293 ± 28 Ma respectively (Fig. 4b). The last best dates the crystallisation of this granodiorite.

Sample 91286417 (lat. 71°28′S, long. 67°41′E), very fine-grained hornblende metadacite, consists of relict altered plagioclase and quartz phenocrysts and has a relict ?flow foliation. It contains green hornblende (~12%), which forms fine-grained aggregates with carbonate, accompanied by minor biotite, chlorite, apatite, and opaque minerals.

Compared with the nearby granitic rocks the metadacite has lower Al_2O_3, K_2O, Rb, and Ba, and higher MgO, CaO, Cr, and Ni. It is markedly Di-normative and has an unfractionated REE pattern (Ce/Y_n = 2.0). A small positive Sr anomaly on its spidergram (Fig. 2) may result from plagioclase accumulation. Associated rocks such as low-K island-arc tholeiites and andesitic to rhyolitic calc-alkaline volcanics are interpreted by Mikhalsky et al. (1996) as evidence of generation at an active continental margin (?Andean type) with an associated island arc.

Zircon grains in the metadacite have diverse morphologies. A few have straight edges, but most are subhedral to anhedral. Their average grainsize is 180 × 110 μm. Most are broken; some have totally ragged margins, yet others are only slightly embayed. Second-order pyramids are present on some terminations. Zoning is uncommon, and there are no obvious cores.

The isotopic data for 91286417 are more scattered than for the other Fisher Massif samples (Fig. 4c). Although this might be partly due to analytical problems (discussed in the Appendix), a geological component of scatter is evident. There is little, if any, correlation of morphology with either isotopic or chemical (U, Th, Th/U) composition of the grains (Table 2) to assist in an interpretation. The most obvious analysis to be discarded from the age calculations is that of grain 15.1, which has an age of about 1900 Ma and must have a xenocrystic origin. Analyses 4.1, 11.1, and 12.1 (shaded in Fig. 4c) plot well below the other analyses, either because they experienced post-crystallisation Pb loss, or because they grew during a subsequent event. The chi-square value of the remaining 16 analyses is 3.4, which indicates a non-ideal grouping. Deletion of four more analyses (2.1, 8.2, 14.1, and 17.1; shaded in Fig. 4c) reduces the value to unity. The removal of these points does not significantly alter the resultant mean age. The remaining 12 analyses yield a concordant data set with pooled $^{206}Pb/^{238}U$, $^{207}Pb/^{235}U$, and $^{207}Pb/^{206}Pb$ ages of 1277 ± 24, 1281 ± 18, and 1283 ± 21 Ma respectively. The spread of both Pb/U ages may signify minor recent Pb loss. Because all the well-preserved grains of igneous appearance are included in the final grouping, the igneous crystallisation of the metadacite is deduced to have occurred at 1283 ± 21 Ma.

Granitic rocks at Mount Collins

Mount Collins, a narrow ridge 13 km long 20 km west of Fisher Massif, is dominated by granitic rocks cut by abundant undeformed tholeiitic dykes. Its principal rock types are pink syenitic granite and quartz monzonite which both grade into darker rocks of charnockitic appearance (though lacking orthopyroxene) and form veins and migmatite in older grey granite. Mafic dykes of at least two generations intrude the granites, and all but the youngest dykes are cut by an association of minor granite sheets, pegmatites, and brittle shear zones.

Sample 91286419, from the eastern end of Mount Collins (lat. 71°29.75′S, long. 66°45′E), is an unfoliated, slightly recrystallised fine to medium-grained grey hornblende–biotite granite (almost a quartz monzonite) that consists of quartz, slightly perthitic microcline (as sparse phenocrysts), oligoclase–andesine, dark brownish green hornblende (4%), dark brown biotite (6%), and minor allanite, zircon, apatite, ilmenite, and magnetite. Sample 91286420, from the same locality, is a medium-grained pink equigranular hornblende–biotite granite which veins and intrudes the grey granite. It is petrographically similar to sample 91286419, but contains more quartz and microcline, and less plagioclase (albite–oligoclase), hornblende (2%), and biotite (2%). Microcline is markedly perthitic, some grains approaching mesoperthite.

Both samples have fractionated spidergrams that evince marked negative Sr anomalies (Fig. 2), typical of granites derived by the melting of an intracrustal source with residual

plagioclase but not garnet. Moderately fractionated Ce/Y_n ratios (11.2 in 91286419, and 10.2 in 91286420) are due to high Ce rather than low Y contents. 91286420 is much more evolved (low MgO, CaO, Ba, and Sr, and high SiO_2), and could have been derived from a less siliceous melt (compositionally resembling 91286419) by the fractionation of plagioclase, apatite, an Fe–Ti oxide, and a ferromagnesian phase. Both are enriched in Zr, Nb, Y, La, and Ce compared with the Fisher Massif granitic rocks, consistent with the high-temperature melting of near-anhydrous granulite-facies source rocks (Sheraton & Black 1988), and both are less visibly altered.

Zircon grains in 91286419 are moderately coarse (averaging 400×150 μm) and of igneous morphology, albeit with rounded terminations. About half of them are euhedrally zoned. Cores (not analysed) are rare. All of the 13 analyses form a statistically simple concordant population with $^{206}Pb/^{238}U$, $^{207}Pb/^{235}U$, and $^{207}Pb/^{206}Pb$ ages of 992 ± 22, 989 ± 20, and 976 ± 25 Ma respectively (Fig. 4d). The intrusion age is considered to be 976 ± 25 Ma.

The moderately coarse elongate zircon grains (averaging 300×130 μm) in 91286420 consist mostly of perfectly euhedral first-order prisms and pyramids. About half of them are clear and homogeneous; the rest display euhedral igneous-type zoning. A few have small, roughly equant cores (not analysed). All 27 isotopic analyses form a statistically simple concordant population with pooled $^{206}Pb/^{238}U$, $^{207}Pb/^{235}U$, and $^{207}Pb/^{206}Pb$ ages of 980 ± 11, 980 ± 8, and 984 ± 7 Ma (Fig. 4e); the last is assumed to be the crystallisation age of this granite.

Sample 91286421 (lat. 71°30.62′S, long. 66°31′E), from the western end of Mount Collins, is a dark medium to coarse-grained, lightly recrystallised, slightly K-feldspar-phyric pyroxene–quartz syenite containing locally sericitised plagioclase (calcic oligoclase). Pyroxene (~7%) in the sample is extensively altered to colourless to pale green clinoamphibole and iddingsite; though the fresher grains are clinopyroxene,

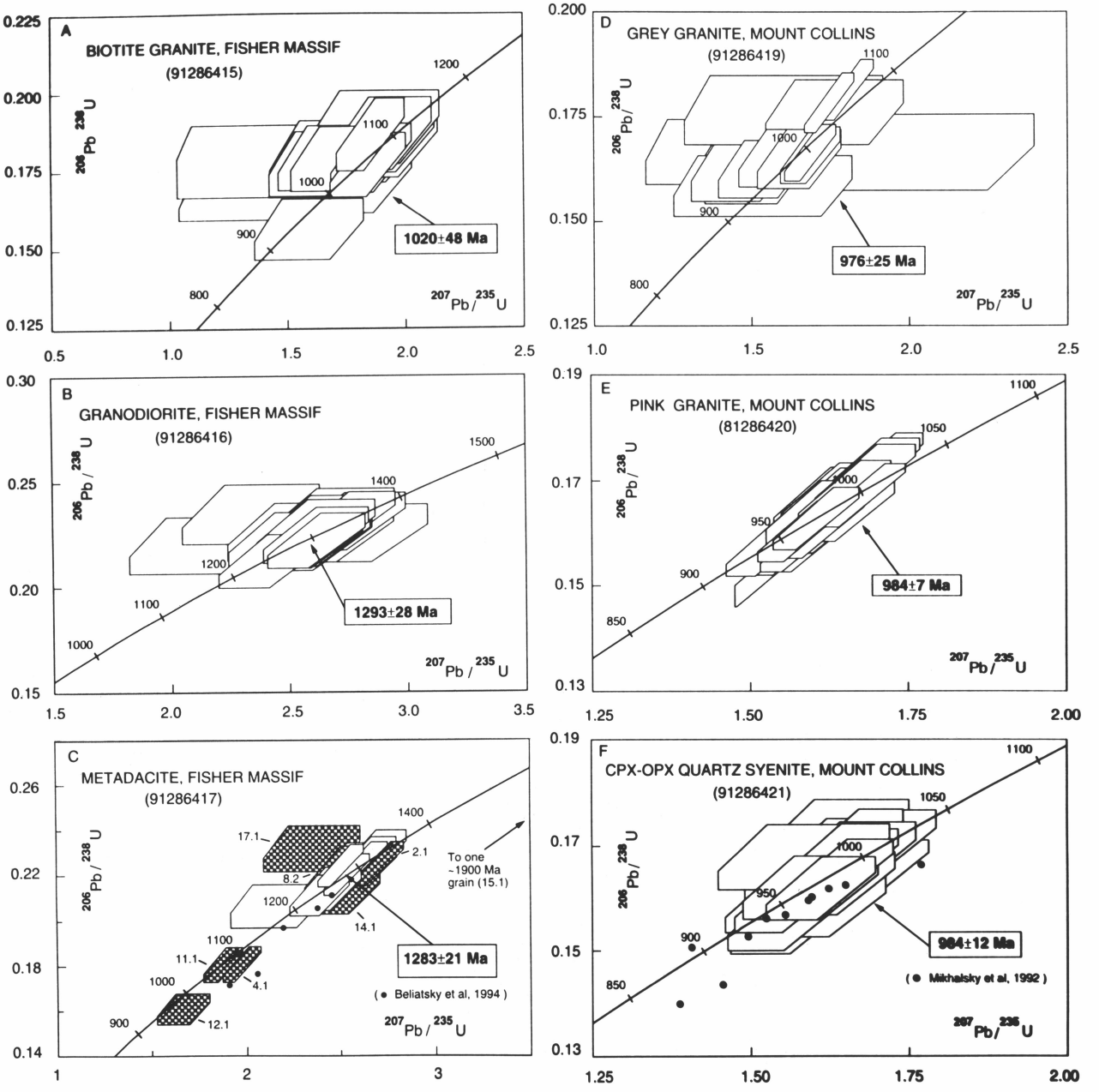

Figure 4. U–Pb concordia diagrams showing SHRIMP data for samples from the Fisher Massif and Mount Collins. Diagram C includes orthodox multigrain data of Beliatsky et al. (1994; filled circles, errors not supplied). Diagram F includes multigrain data of Mikhalsky et al. (1992; filled circles, errors in Pb/U ratios not supplied). SHRIMP error boxes reflect 95% confidence limits.

some of the intensely altered ones might have been orthopyroxene. Zircon is unusually abundant in the rock, which also contains small amounts of biotite, hornblende, ilmenite, magnetite, apatite, and carbonate. Other rocks from the same area grade into monzonite and quartz monzonite, which generally contain more hornblende and, to a lesser extent, biotite. Some of the hornblende forms sieve-like aggregates with quartz, possibly replacing pyroxene. Partly altered clinopyroxene locally exhibits exsolution textures. Allanite is a significant accessory mineral in some of these rocks, and all have abundant zircon.

The quartz syenite (91286421) is unrelated to the granites analysed from the eastern end of Mount Collins; it has lower MgO, Th, Cr and Ni, and higher Ba and Zr (allowing for different SiO_2 contents). Its spidergram is unusual in showing a pronounced positive Zr anomaly, as well as Ba and K anomalies, but there are no corresponding enrichments in REE, Nb, Y, or Ga (Fig. 2). The rock does not, therefore, have the compositional features (other than high Zr) of A-type ('anorogenic') intrusions (Collins et al. 1982). This is not surprising, as the intrusion is evidently syn- to late metamorphic in age. Fractionation of an alkali basalt magma, probably with some degree of crustal assimilation, was suggested by Zhao et al. (1995) for the Cambrian Yamato syenite of Dronning Maud Land. However, the high Zr and lack of a negative Sr anomaly (as well as a large positive Eu anomaly) in an otherwise highly evolved (low *mg*, Ni and Cr) rock suggest that the Mount Collins syenite is a feldspar- (and zircon-) rich cumulate.

Zircons in this rock are moderately fine-grained (averaging 100×50 μm), optically clear, unzoned, and of obvious original igneous morphology, though no sharp terminations remain. All 29 isotopic analyses define a simple statistical population with concordant $^{206}Pb/^{238}U$, $^{207}Pb/^{235}U$, and $^{207}Pb/^{206}Pb$ ages of 982 ± 11, 981 ± 9, and 984 ± 12 Ma, of which the last defines the crystallisation age (Fig. 4f). The ages of all three analysed samples from Mount Collins are thus indistinguishable.

Paragneiss at Mount Meredith

The southeastern side of Mount Meredith is composed principally of coarse-grained, pegmatite-banded biotite–quartz–feldspar gneiss. Though non-diagnostic, assemblages and textures suggest this rock was metamorphosed to the amphibolite facies. Sample 91286412 (lat. 71°15.5′S, long. 67°42′E), a granoblastic inequigranular interlobate-textured fine to medium-grained gneiss, has a prominent foliation defined by oriented biotite grains. Rich in quartz (~37%) and sodic andesine (~53%), it contains only minor, slightly perthitic orthoclase (~2%), dark brown biotite (6%, partly altered to bright green pleochroic chlorite), muscovite (1%), and minor apatite, zircon, monazite, and opaque minerals. Retrograde patches contain chlorite, sericite, and a little epidote. Sample 91286413, from a more quartzofeldspathic layer twenty metres up-section from and petrographically similar to 91286412, contains much more quartz (~70%), less plagioclase (sericitised oligoclase, 25%) and biotite (4%), but little or no K-feldspar.

The Mount Meredith samples are probably of sedimentary origin. The normative Q/(Q+Ab+Or) ratio (52%) of sample 91286412 is much higher than in typical felsic igneous rocks, and quartz-rich 91286413 presumably represents a metamorphosed impure sandstone or quartzite (i.e. a psammite). Both samples have fractionated spidergrams that show marked Nb, Sr, P, and Ti depletion (Fig. 2), typical of clastic sedimentary rocks (Tarney et al. 1987). 91286413 is more depleted in most incompatible elements, particularly Ba, consistent with its very low K-feldspar content. Moderately high Zr in both rocks suggests the presence of detrital zircon. Somewhat surprisingly, neither sample is very peraluminous, implying derivation from immature sedimentary rocks. Their K/Na ratios suggest the rocks were derived from a K-poor source, like some Archaean hornblende–biotite gneisses of the southern PCM (J.W. Sheraton, unpublished data).

Most zircon grains in 91286412 are about 200 μm long, and have elongation ratios between 2:1 and 3:1. The morphology of the more euhedral grains indicates a magmatic origin, although most have been rounded, and some pitted by subsequent sedimentary processes. Some grains are zoned; others are optically homogeneous. Some have cores, but the enclosing rims are too narrow (just a few microns) to be analysed.

Zircon grains in 91286413 are on average slightly larger than those in 91286412, and appear to constitute two morphological types: one comprises grains resembling but somewhat more rounded than those in 91286412; in the other type, the grains are more equant (elongation ratios 1:1 to 2:1), multifaceted, and invariably homogeneous.

Similar populations of Archaean and Proterozoic zircons occur in both samples (Fig. 3d). The Archaean grains range in $^{207}Pb/^{206}Pb$ age from about 2800 Ma to 2500 Ma. A distinct hiatus separates that group from the Proterozoic zircons, which range from 2100 Ma to 1800 Ma old. There is a suggestion that the Archaean group might represent three discrete populations at about 2500, 2650–2700, and ca 2800 Ma, but differentiating age groups among the Proterozoic grains requires a higher degree of speculation. Both morphological types of zircon in the more leucocratic sample exhibit a similar range of ages.

Overgrowths on three zircons from the more quartzofeldspathic sample were found to have much higher U contents (>1000 ppm) than the cores (<200 ppm) they enclose. Two rims (24.2 and 30.2) yielded similar ages of about 1670 Ma, despite their contrasting core ages (24.1 Archaean, 30.1 Proterozoic), and the other analysed rim (16.2) was about 100 Ma younger; all three are somewhat discordant. The overgrowths are similarly structured: each has inner and outer growth zones separated by a thin, more brightly cathodoluminescent layer, from which one might infer that they were generated by the same event — although it is not clear whether that event produced the present banded gneiss or an antecedent.

Discussion

Orthopyroxene-bearing quartz monzonite from Loewe Massif and quartz syenite from Mount Collins have yielded identical ages of 980 ± 21 and 984 ± 12 Ma (Table 3), implying that they formed during widespread magmatism that accompanied regional high-grade metamorphism. Mount Collins is the southernmost pyroxene-bearing intrusion, and Loewe Massif the largest. Intrusive charnockitic rocks are common in this part of East Antarctica; they also occur at several places in the Porthos Range (Munksgaard et al. 1992), in the Reinbolt Hills area (140 km east of Jetty Peninsula; Nichols & Berry 1991), around Mawson Station on the Mac.Robertson Land coast (Young & Black 1991), and at many other localities. Previously reported dates are similar to those reported here. For example, zircons from the Mawson charnockite dated by Young & Black (1991) using SHRIMP yielded indistinguishable crystallisation ages of 985 ± 29 and 954 ± 2 Ma.

The charnockitic intrusives postdate the dominant flat-lying structures of the northern PCM (D_3 of Fitzsimons & Thost 1992). D_3 most likely developed during the earlier stages of the ca 1000-Ma metamorphic episode. Later upright fold and shear structures (D_{5-8} of Fitzsimons & Thost 1992) postdate the intrusions and leucogneiss bodies, but the interval may be short. An imprecise Rb–Sr isochron age of 880 ± 140 Ma for the Porthos Range charnockites (Hensen et al. 1992) suggests that no younger (e.g., 500-Ma) high-grade tectonothermal events have affected these rocks.

Having zircon populations that are simple and isotopically concordant to within error, the three analysed granitic rocks

Table 3. Summary of SHRIMP zircon ages from the northern Prince Charles Mountains.

Sample (prefix 912864)	*Locality*	*Lithology*	$^{207}Pb/^{206}Pb$ *age ± ts*	$^{206}Pb/^{238}U$ *age ± ts*	*± Inheritance*
07	Loewe Massif	Quartz monzonite	980 ± 21	944 ± 41	
19	Mount Collins	Granite	976 ± 25	992 ± 22	
20	Mount Collins	Granite	984 ± 7	980 ± 11	
21	Mount Collins	Quartz syenite	984 ± 12	982 ± 11	
03	Mount McCarthy	Leucogneiss	990 ± 30	963 ± 100*	~1850 Ma
15	Fisher Massif	Granite	1020 ± 48	1056 ± 24	
16	Fisher Massif	Granodiorite	1293 ± 28	1309 ± 29	
17	Fisher Massif	Metadacite	1283 ± 21	1277 ± 24	~1900 Ma
12/13	Mount Meredith	Felsic gneiss	2800–2500, 2100–1800 Ma detrital populations		

* Error multiplication by 2.8 to account for residual scatter.

from Mount Collins are essentially coeval at ca 980 Ma. Our data, therefore, contrast with the conventional bulk-zircon data of Mikhalsky et al. (1992) for three syenitic granites from Mount Collins. Mikhalsky et al. (1992) obtained a cluster of near-concordant points between 900 and 1000 Ma, plus a number of more discordant points with younger ages, and two discordant points from one sample (34341) with older $^{207}Pb/^{206}Pb$ ages (cf. Fig. 4f). By extrapolating to concordia through these exceptional discordant points, Mikhalsky et al. (1992) deduced a crystallisation age of 1400 ± 80 Ma for all three samples and later disturbances between 700 and 900 Ma. Our results, however, suggest that crystallisation at ca 980 Ma was much more likely. Sample 34341, which gave the older apparent ages probably contains some inherited zircon, while the more highly discordant points in the other samples might reflect partial Pb loss in recent times. We can see no evidence for a disturbance at ca 700 Ma (cf. Mikhalsky et al. 1992).

Our results from Fisher Massif support the conclusions of Beliatsky et al. (1994), based on bulk zircon data, regarding the age of the metavolcanic sequence there. Our metadacite sample contained zircons of diverse morphology: a concordant ca 1280 Ma population with some excess scatter in age suggesting a non-ideal grouping; one clearly inherited grain with a minimum age of ca 1900 Ma; and three analyses with younger apparent ages of ca 1100 Ma, which might reflect lost Pb (? at 1000 Ma). From these data, we have interpreted the volcanic eruption age to be 1283 ± 21 Ma, which also coincides with our age estimate for the nearby granodiorite (1293 ± 28 Ma). Beliatsky et al.'s (1994) pooled fractions (shown in Fig. 4c for comparison) form a similar array of points indicating intrusion ca 1300 Ma, plus one sample with a major inherited component (offscale). The extrapolated lower intercept ages of these bulk discordia (364 ± 16 and –63 ± 68 Ma) probably are not geologically significant.

The new data for Fisher Massif and Mount Collins also provide important age constraints on the mafic dykes in the area. These had been previously correlated with metadolerite dyke swarms in the southern PCM (Tingey 1982), believed to be of Mesoproterozoic age on the basis of their geochemical similarity to dated dyke suites in the Vestfold Hills and Enderby Land (Sheraton & Black 1981). However, the geochemistry of the northern PCM dyke suites is not consistent with such a correlation (J.W. Sheraton, unpublished data), and indicates different origins for the Mount Collins dykes and the Fisher Massif–Mt Willing group (e.g., much lower Nb/Zr in the Fisher Massif dykes). Our isotopic results support this distinction and show that the Fisher Massif dykes are between 1290 and 1020 Ma old (i.e. bracketed by the ages of the two analysed granites), whereas the Mount Collins dykes are younger than 980 Ma. In comparison, the tholeiitic suites in the Vestfold Hills, which have been correlated with the southern PCM metadolerites, are now known to have been emplaced in separate events at ca 1380 and 1240 Ma (Lanyon et al. 1993). Such local and regional differences may assist with terrane reconstructions.

The isotopic ages presented in this paper do not address directly the question of the original protolith ages of the northern PCM basement orthogneisses affected by the ca 1000-Ma tectonothermal episode. However, some indication of basement ages is recorded in the minor inherited zircon in two of the samples: one ca 1900-Ma grain in the Fisher Massif metadacite, and the two ca 1850-Ma cores in the locally derived Mount McCarthy leucogneiss. A felsic xenolith from the Mawson charnockite studied by Young & Black (1991) contains many zircons in this age range, which is well represented also in the detrital zircon population analysed from the Mount Meredith paragneiss. The Mount Meredith suite also includes a late Archaean population (2500 to 2800 Ma), perhaps derived from the southern PCM terranes. Additionally, analyses of zircon rims from the Mount Meredith suite and also from the Mount McCarthy inherited zircons, suggest a possible metamorphic event at ca 1650 Ma. The absence of zircons in the age range 1300 to 1000 Ma from the paragneiss implies that its sedimentary precursor accumulated before the other rocks dated in this study were emplaced.

Model ages (1070–1320 Ma) derived from previously compiled initial Sr ratios for northern PCM orthogneisses (Tingey 1991) imply relatively short crustal residence times for their precursors, but could also reflect the effects of disturbance at ca 1000 Ma. Nd-depleted-mantle (DM) model ages, which may be more reliable, extend as far back as 2000 Ma (S.-s. Sun, unpublished data).

These results will also influence the current debate on the nature and extent of the 500-Ma metamorphic episode in East Antarctica. At present, the only rock in the northern PCM known to have formed 500 Ma ago is the Jetty Peninsula pegmatite analysed by Manton et al. (1992). None of the zircon populations analysed in this study includes a 500-Ma component either in the form of younger rims, as separate zircon populations, or as the lower intercept of Pb-loss discordia. Most of our data are concordant to within error, and the few exceptions show no clear discordance trends — like the zircon populations of the basement gneisses of the Vestfold Hills on the Prydz Bay coast (Black et al. 1991), but in marked contrast to those of the nearby Rauer Islands (Kinny et al. 1993) and Larsemann Hills (Zhao et al. in press), which show major effects of 500-Ma events on the zircon isotopic systematics. Furthermore, large (>1 km) granite bodies were emplaced in the Mawson Escarpment (southern PCM) and eastern Amery Ice Shelf areas at about this time (Sheraton & Black 1988; Tingey 1991).

Tingey (1982, 1991) interpreted the 500-Ma event in the northern PCM as the time of a low-grade 'pervasive heating event' which reset Rb–Sr mineral systems (biotite, muscovite). Hand et al. (1994), by contrast, assigned this event to probable upper-amphibolite-facies metamorphism on Else Platform. Zhou & Hensen (1995) obtained ca 500-Ma Sm–Nd ages from garnets in rocks from Mount McCarthy (including the leucogneiss, which yielded 990-Ma zircons in our study). The regional significance of these results is not yet clear. Certainly on Fisher Massif, there is no indication of metamorphic grade ever having advanced beyond the lower amphibolite facies, and textures of the <980 Ma tholeiitic dykes on Mount Collins are intergranular to gabbroic (i.e., igneous).

Conclusion

Two important episodes of magmatism in the northern PCM occurred at 1300–1280 Ma (Fisher Massif–Mount Willing area) and at 1020–980 Ma. The ca 1300-Ma episode involved multiple intrusions of mafic to felsic magmas in the southern part of the region, and extrusion of a major volcanic pile on Fisher Massif. The ca 1000-Ma episode involved the widespread intrusion of granitic magmas (orthopyroxene-bearing quartz monzonite, granite, and syenitic granite) representing a combination of both mantle-derived and intracrustal melts. These intrusions were accompanied by granulite-facies metamorphism, local partial melting of the country rock gneisses, and the formation of minor leucogneiss bodies, except on Fisher Massif, where a biotite granite pluton was emplaced at this time under lower-amphibolite-facies conditions. The Fisher Massif volcanics have never been metamorphosed beyond the lower amphibolite facies and appear to represent a remnant of originally higher-level crust than the rocks now exposed to the north and west (e.g., Mount Collins), or even a distinct microplate.

Later additions to the northern PCM crust are few. They include: the intrusion on Jetty Peninsula of minor granitic stocks and dykes at ca 940 Ma and of pegmatites at ca 500 Ma (Manton et al. 1992); emplacement of tholeiitic dykes at Mount Collins (<980 Ma) and alkaline dykes of various ages (Sheraton 1983); and deposition of Permian sediments in the Beaver Lake area (Fig. 1) associated with the development of the Lambert Rift. Overall, the 500-Ma metamorphic episode, which is prominent elsewhere in East Antarctica, appears to have been of relatively minor importance in the northern PCM because it affected only some mineral systems.

Acknowledgments

Fieldwork by PDK was funded by a grant from the Antarctic Science Advisory Council. Our thanks to all members of the ANARE 1990–91 PCM expedition, particularly W. Crowe, I. Scrimgeour, N. Williams, and P. Colpo for assistance in sample collection; to AGSO technicians C. Foudoulis, J. Pyke, K. Armstrong, L. Keast, W. Pappas, and E. Webber; and to R.J. Tingey and C.M. Fanning for helpful reviews of the paper.

References

Arriens, P., 1975. The Precambrian geochronology of Antarctica. In: First Australian Geological Convention, Adelaide. Geological Society of Australia, Abstracts, 97–98.

Beliatsky, B.V., Laiba, A.A. & Mikhalsky, E.V., 1994. U–Pb zircon age of the metavolcanic rocks of Fisher Massif (Prince Charles Mountains, East Antarctica). Antarctic Science, 6, 355–358.

Black, L.P., Kinny, P.D., Sheraton, J.W. & Delor, C.P., 1991. Rapid production and evolution of late Archaean felsic crust in the Vestfold Block of East Antarctica. Precambrian Research, 50, 283–310.

Champion, D.C. & Sheraton, J.W., 1993. Geochemistry of granitoids of the Leonora–Laverton region, Eastern Goldfields Province. In: Williams, P.R. & Haldane, J.A. (editors), An international conference on crustal evolution, metallogeny and exploration of the Eastern Goldfields. Extended abstracts. Australian Geological Survey Organisation, Record 1993/94, 39–46.

Chappell, B.W. & White, A.J.R., 1974. Two contrasting granite types. Pacific Geology, 8, 173–174.

Compston, W., Williams, I.S. & Meyer, C., 1984. U–Pb geochronology of zircons from lunar breccia 73217 using a sensitive high mass-resolution ion microprobe. Journal of Geophysical Research, 89, B525–534.

Compston, W., Williams, I.S., Kirschvink, J.L., Zichao, Z. & Guogan, M., 1992. Zircon U–Pb ages for the Early Cambrian time-scale. Journal of the Geological Society, London, 149, 171–184.

Collins, W.J., Beams, S.D., White, A.J.R. & Chappell, B.W., 1982. Nature and origin of A-type granites with particular reference to southeastern Australia. Contributions to Mineralogy and Petrology, 80, 189–200.

Crowe, W., 1994. Geology, metamorphism, and petrogenesis of the Fisher Terrane, Prince Charles Mountains, East Antarctica. MSc thesis, Australian National University, Canberra (unpublished).

Cruikshank, B.I. & Pyke, J.G., 1993. Analytical methods used in Mineral and Land Use Program's geochemical laboratory. Australian Geological Survey Organisation, Record 1993/26.

Cumming, G.L. & Richards, J.R., 1975. Ore lead isotopes in a continuously changing Earth. Earth and Planetary Science Letters, 28, 155–171.

DePaolo, D.J., 1981. Trace element and isotopic effects of combined wallrock assimilation and fractional crystallisation. Earth and Planetary Science Letters, 53, 189–202.

Fedorov, L.V., Zatsepin, E.N. & Leichenkov, G.L., 1987. Geology of the Fisher Massif. Abstract, International Symposium on Antarctic Earth Sciences, Cambridge, UK, 42.

Fitzsimons, I.C.W. & Thost, D.E., 1992. Geological relationships in high-grade basement gneiss of the northern Prince Charles Mountains, East Antarctica. Australian Journal of Earth Sciences, 39, 173–193.

Hand, M., Scrimgeour, I., Stüwe, K., Arne, D. & Wilson, C.J.L., 1994. Geological observations in high-grade mid-Proterozoic rocks from Else Platform, northern Prince Charles Mountains region, East Antarctica. Australian Journal of Earth Sciences, 41, 311–329.

Hensen, B.J., Munksgaard, N.C. & Thost, D.E., 1992. Geochemistry and geochronology of Proterozoic granulites from the northern Prince Charles Mountains, East Antarctica. ANARE Research Notes, 85, 9.

Hofmann, J., 1991. Fault tectonics and magmatic ages in the Jetty Oasis area, Mac.Robertson Land: a contribution to the Lambert rift development. In: Thomson, M.R.A. et al. (editors), Geological evolution of Antarctica. Cambridge University Press, UK, 107–112.

Kamenev, E., Andronikov, A.V., Mikhalsky, E.V., Krasnikov, N.N. & Stüwe, K., 1993. Soviet geological maps of the Prince Charles Mountains, East Antarctic Shield. Australian Journal of Earth Sciences, 40, 501–517.

Kinny, P.D., Black, L.P. & Sheraton, J.W., 1993. Zircon ages and the distribution of Archaean and Proterozoic rocks in the Rauer Islands. Antarctic Science, 5, 193–206.

Lanyon, R., Black, L.P. & Seitz, H.-M., 1993. U–Pb zircon dating of mafic dykes and its application to the Proterozoic geological history of the Vestfold Hills, East Antarctica. Contributions to Mineralogy and Petrology, 115, 184–203.

McKelvey, B.C. & Stephenson, N.C.N., 1990. A geological reconnaissance of the Radok Lake area, Amery Oasis, Prince Charles Mountains. Antarctic Science, 2, 53–66.

Manton, W.I., Grew, E.S., Hofmann, J. & Sheraton, J.W., 1992. Granitic rocks of the Jetty Peninsula, Amery Ice Shelf area, East Antarctica. In: Yoshida, Y. (editor), Recent progress in Antarctic Earth science. Terra Scientific Publishing Co., Tokyo, 179–189.

Mikhalsky, E.V., Andronikov, A.V. & Beliatsky, B.V., 1992. Mafic igneous suites in the Lambert Rift Zone. In: Yoshida, Y. (editor), Recent progress in Antarctic Earth science. Terra Scientific Publishing Co., Tokyo, 173–178.

Mikhalsky, E.V., Sheraton, J.W., Laiba, A.A. & Beliatsky, B.V., 1996. Geochemistry and origin of Mesoproterozoic metavolcanic rocks of Fisher Massif, Prince Charles Mountains, East Antarctica. Antarctic Science, 8, 85–104.

Munksgaard, N.C., Thost, D.E. & Hensen, B.J., 1992. Geochemistry of Proterozoic granulites from northern Prince Charles Mountains, East Antarctica. Antarctic Science, 4, 59–69.

Nichols, G.T. & Berry, R.F., 1991. A decompressional P–T path, Reinbolt Hills, East Antarctica. Journal of Metamorphic Geology, 9, 257–266.

Norrish, K. & Chappell, B.W., 1977. X-ray fluorescence spectrometry. In: Zussman, J. (editor), Physical methods in determinative mineralogy. Academic Press, London, 201–272.

Norrish, K. & Hutton, J.T., 1969. An accurate X-ray spectrographic method for the analysis of a wide range of geological samples. Geochimica et Cosmochimica Acta, 33, 431–453.

Sheraton, J.W., 1983. Geochemistry of mafic igneous rocks of the northern Prince Charles Mountains, Antarctica. Journal of the Geological Society of Australia, 30, 295–304.

Sheraton, J.W. & Black, L.P., 1981. Geochemistry and geochronology of Proterozoic dykes of East Antarctica: evidence for mantle metasomatism. Contributions to Mineralogy and Petrology, 78, 305–317.

Sheraton, J.W. & Black, L.P., 1988. Chemical evolution of granitic rocks in the East Antarctic Shield, with particular reference to post-orogenic granites. Lithos, 21, 37–52.

Sheraton, J.W. & England, R.N., 1980. Highly potassic mafic dykes from Antarctica. Journal of the Geological Society of Australia, 27, 129–135.

Sheraton, J.W., Tindle, A.G. & Tingey, R.J., 1996. Geochemistry, origin and tectonic setting of granitic rocks of the Prince Charles Mountains, Antarctica. AGSO Journal of Australian Geology & Geophysics, 16(3), 345–370.

Steiger, R.H. & Jäger, E., 1977. Subcommission on geochronology: convention on the use of decay constants in geo- and cosmochronology. Earth and Planetary Science Letters, 36, 359–362.

Sun, S.-s. & McDonough, W.F., 1989. Chemical and isotopic systematics of oceanic basalts: implications for mantle composition and processes. In: Saunders, A.D. & Norry, M.J. (editors), Magmatism in the ocean basins. Geological Society, Special Publication, 42, 313–345.

Tarney, J., Wyborn, L.E.A., Sheraton, J.W. & Wyborn, D., 1987. Trace element differences between Archaean, Proterozoic and Phanerozoic crustal components — implications for crustal growth processes. In: Ashwal, L.D. (editor), Workshop on the growth of continental crust. Lunar and Planetary Institute, Technical Report 88.02, 139–140.

Tingey, R.J., 1982. The geologic evolution of the Prince Charles Mountains — an Antarctic Archean cratonic block. In: Craddock, C. (editor), Antarctic geoscience. University of Wisconsin Press, Madison, 455–464.

Tingey, R.J., 1991. The regional geology of Archaean and Proterozoic rocks in Antarctica. In: Tingey, R.J. (editor), The geology of Antarctica. Oxford University Press, UK, 1–73.

Watson, E.B. & Harrison, T.M., 1983. Zircon saturation revisited: temperature and composition effects in a variety of crustal magma types. Earth and Planetary Science Letters, 64, 295–304.

Yakovlev, B.G., Ol'khovik, Yu.A., Litvin, A.L., Lavrov, P.I. & Semenov, V.S., 1986. Physico-chemical conditions of metamorphic development in the enderbite–gneiss complex of Mac.Robertson Land (East Antarctica). Mineralogicheskiy Zhurnal, 8(6), 20–34 (in Russian).

Young, D.N. & Black, L.P., 1991. U–Pb zircon dating of Proterozoic igneous charnockites from the Mawson Coast, East Antarctica. Antarctic Science, 3, 205–216.

Zhao, J.-X., Shiraishi, K., Ellis, D.J. & Sheraton, J.W., 1995. Geochemical and isotopic studies of syenites from the Yamato Mountains, East Antarctica: implications for the origin of syenitic magmas. Geochimica et Cosmochimica Acta, 59, 1363–1382.

Zhao, Y., Song, B., Zhang, Z., Fu, Y., Chen, T., Wang, Y., Ren, L., Yao, Y., Li, J. & Liu, X., in press. Early Paleozoic ("Pan-African") thermal event of the Larsemann Hills and its neighbours, Prydz Bay, East Antarctica. Precambrian Research.

Zhou, B. & Hensen, B.J., 1995. Inherited Sm/Nd isotope components preserved in monazite inclusions within garnets in leucogneiss from East Antarctica. Chemical Geology, 121, 317–326.

Appendix

Analytical notes

All samples were chemically analysed (Table 1) in the AGSO laboratory. FeO was determined volumetrically, LOI (loss on ignition) gravimetrically, and Li by atomic absorption spectrophotometry. All the remaining elements were determined by X-ray fluorescence spectrometry according to the methods of Norrish & Hutton (1969) and Norrish & Chappell (1977). Further details of methods and accuracy are presented by Cruikshank & Pyke (1993).

Zircons were separated by standard heavy liquid and magnetic procedures, and then by hand-picking. They were then mounted in epoxy resin discs along with fragments of the SL13 standard zircon. The discs were polished and Au-coated before they were analysed on the SHRIMP I ion-microprobe at the Research School of Earth Sciences, Australian National University, Canberra. (Samples 91286412 and 13 were analysed under similar conditions on the SHRIMP II at the Western Australia Isotope Science Research Centre, Perth.) A primary beam of singly, negatively charged oxygen was used to sputter positive secondary ions from areas of ca 25-μm diameter in individual sectioned zircons. Zr_2O^+, $^{204}Pb^+$, background (baseline) near $^{204}Pb^+$, $^{206}Pb^+$, $^{207}Pb^+$, $^{208}Pb^+$, $^{238}U^+$, ThO^+ and UO^+ were measured in cycles by magnetic-field switching, seven cycles per data set. Operating at a mass resolution >6500 facilitated the removal of significant spectral interferences (Compston et al. 1984). Discrimination between the Pb isotopes was negligible. Differential fractionation between U and Pb was monitored by reference to a $^{206}Pb/^{238}U$ ratio of 0.0928 (equivalent to an age of 572 Ma) for the SL13 zircon standard during interspersed analyses based on a power-law ($^{206}Pb^+/^{238}U^+ = a[^{238}UO^+/^{238}U^+]^2$) relationship. The precision of the Pb/U ratios of the unknowns is augmented

by the precision of $^{206}Pb/^{238}U$ for the standard (these ranged from 1.8% to 3.0%) during each relevent session. The factor 'f' for converting the measured $^{232}ThO^+/^{238}U^+$ ratios to $^{232}Th/^{238}U$ is derived from the linear relationship $f = 0.03446.^{238}UO^+/^{238}U^+ + 0.8680$. Radiogenic Pb compositions were determined after subtracting contemporaneous common Pb (Cumming & Richards 1975).

All reported ages represent $^{207}Pb/^{206}Pb$ data that have been corrected by the ^{204}Pb technique (Compston et al. 1984). However, this procedure had to be modified for deriving the composition (and age) of sample 91286417, because a slight offset from the normal magnetic-field settings for the 207 and 208 peaks had occurred during the analysis of this sample. On the basis of an atypical composition of the standard zircon fragment, this bias was estimated to be 2.7 per cent, and was added to both the 207 and 208 count rates. The same fragment of the standard showed no such bias during the analysis of samples 91286415 and 91286416, confirming that it could be meaningfully used to assess non-ideal instrument conditions.

Ages have been calculated from the U and Th decay constants recommended by Steiger & Jäger (1977). Their uncertainties are expressed at the 95% ($t\delta$) confidence level, and so are the precision fields for each analysis in the concordia diagrams. In contrast, 1-σ precision limits are cited in Table 2.